Cell

The Angelman Syndrome Protein Ube3A Regulates Synapse Development by Ubiquitinating Arc

Paul L. Greer,[1,2,6] Rikinari Hanayama,[1,6] Brenda L. Bloodgood,[1] Alan R. Mardinly,[1] David M. Lipton,[1] Steven W. Flavell,[1] Tae-Kyung Kim,[1] Eric C. Griffith,[1] Zachary Waldon,[5] Rene Maehr,[4] Hidde L. Ploegh,[4] Shoaib Chowdhury,[3] Paul F. Worley,[3] Judith Steen,[5] and Michael E. Greenberg[1,*]

[1]Department of Neurobiology, Harvard Medical School, 220 Longwood Avenue, Boston, MA 02115, USA
[2]Program in Biological and Biomedical Sciences, Harvard Medical School, 300 Longwood Avenue, Boston, MA 02115, USA
[3]Department of Neuroscience, The Johns Hopkins University School of Medicine, Baltimore, MD 21205, USA
[4]Whitehead Institute for Biomedical Research, Cambridge, MA 02142, USA
[5]F.M. Kirby Neurobiology Center and Department of Neurology, Children's Hospital Boston, MA 02115, USA
[6]These authors contributed equally to this work
*Correspondence: meg@hms.harvard.edu
DOI 10.1016/j.cell.2010.01.026

SUMMARY

Angelman Syndrome is a debilitating neurological disorder caused by mutation of the E3 ubiquitin ligase *Ube3A*, a gene whose mutation has also recently been associated with autism spectrum disorders (ASDs). The function of Ube3A during nervous system development and how Ube3A mutations give rise to cognitive impairment in individuals with Angleman Syndrome and ASDs are not clear. We report here that experience-driven neuronal activity induces *Ube3A* transcription and that Ube3A then regulates excitatory synapse development by controlling the degradation of Arc, a synaptic protein that promotes the internalization of the AMPA subtype of glutamate receptors. We find that disruption of Ube3A function in neurons leads to an increase in Arc expression and a concomitant decrease in the number of AMPA receptors at excitatory synapses. We propose that this deregulation of AMPA receptor expression at synapses may contribute to the cognitive dysfunction that occurs in Angelman Syndrome and possibly other ASDs.

INTRODUCTION

Angelman Syndrome (AS) is a neurodevelopmental disorder characterized by motor dysfunction, severe mental retardation, speech impairment, seizures, and a high prevalence of autism (Williams et al., 2006). Genetic studies revealed that AS is associated with maternal deletions of chromosome 15q11-q13, paternal chromosome 15 uniparental disomy, or rare imprinting defects that affect the transcription of genes within 15q11-q13 (Clayton-Smith and Laan, 2003). Recent studies indicate that failure to inherit a normal maternal copy of the *UBE3A* gene (which resides within 15q11-q13) accounts for 85%–90% of AS cases, and specific loss-of-function mutations in human *UBE3A* have been identified in a subset of affected individuals (Kishino et al., 1997; Matsuura et al., 1997).

The role of *Ube3A* mutations in AS is supported by targeted inactivation of *Ube3a* in mice (Jiang et al., 1998; Miura et al., 2002). Upon inheritance of the mutation through the maternal germline, the mutant mice display features of AS. The finding that imprinting of *Ube3A* occurs in specific brain regions reinforces the idea that loss of Ube3A function in the nervous system underlies AS (Jiang et al., 1998; Albrecht et al., 1997).

The study of *Ube3A* mutations also provides insight into the causes of autism. Autism spectrum disorders (ASDs) are complex disorders characterized by impairment in social interactions and the occurrence of repetitive behaviors. Despite the high prevalence of ASDs, little is known about the etiology of these disorders. Nonetheless, there is a significant genetic component to ASDs, and thus considerable effort has gone into identifying genetic mutations that cause ASDs. These studies suggest that *Ube3A* is a candidate ASD gene. Abnormalities within chromosomal region 15q11-q13 are among the most prevalent mutations identified in ASDs, accounting for 1%–2% of all ASD cases (Sutcliffe et al., 2003; Cook et al., 1997). Recent reports indicate that copy number variance within the *Ube3A* locus is associated with autism (Glessner et al., 2009).

Despite the critical role that Ube3A plays in human cognitive function, little is known about Ube3A's contribution to nervous system development or how the mutation of *Ube3A* leads to cognitive impairment. Electrophysiological experiments have demonstrated impaired long-term potentiation (LTP) in *Ube3A* knockout mice (Jiang et al., 1998). Additionally, a recent study implicates Ube3A in experience-dependent plasticity (Yashiro et al., 2009). While these experiments demonstrate a crucial role for Ube3A in synaptic transmission, the mechanisms by which Ube3A regulates synaptic function are poorly understood. Possible insight into how Ube3A functions may come from the finding that Ube3A is a member of the E3 ubiquitin ligase family

of enzymes, a class of proteins that catalyzes the addition of ubiquitin moieties to target substrates, often leading to the degradation of the ubiquitinated protein. Genetic studies indicate that the ubiquitin ligase activity of Ube3A is necessary for normal human cognitive function inasmuch as disruption of this activity leads to AS (Cooper et al., 2004). Nevertheless, the neuronal substrates of Ube3A that mediate its effects on synaptic function remain unknown.

In this study, we sought to understand how disruption of Ube3A results in synaptic dysfunction. We find that Ube3A is a neuronal activity-regulated protein that controls synaptic function by ubiquitinating and degrading the synaptic protein Arc. In the absence of Ube3A, elevated levels of Arc accumulate in neurons, resulting in the excessive internalization of AMPA receptors (AMPARs) at synapses and impaired synaptic function. This impaired AMPAR trafficking may be a cause of the cognitive dysfunction that occurs in AS. These findings suggest potential therapeutic targets for treating AS, a disorder for which there is currently no effective therapy.

RESULTS

Activity-Dependent Regulation of Ube3A

One clue as to how Ube3A might function in nervous system development comes from the observation that the symptoms of AS and ASDs first become apparent within the first years of a child's life (Williams et al., 2006), during which sensory experiences play a key role in shaping neuronal connectivity. The effect of environmental cues on cognitive development is mediated in part by the release of glutamate at excitatory synapses. This triggers a program of gene expression that plays a critical role in synapse development (Greer and Greenberg, 2008). We considered the possibility that AS may arise from a deficit in activity-dependent regulation of Ube3A.

We find that the expression of *Ube3A* messenger RNA (mRNA) in cultured neurons is significantly increased by either membrane depolarization or glutamate receptor activation (Figure 1A). Conversely, blocking neuronal activity with inhibitors of NMDARs, AMPARs and sodium channels results in a decrease in *Ube3A* mRNA expression (Figure S1A available online). Ube3A protein levels mirror the change in mRNA level under these conditions (Figure 1B and Figures S1B and S1C).

We next asked whether *Ube3A* expression is induced by neuronal activity in the intact mouse brain. During kainate-induced seizures, *Ube3A* mRNA and protein levels are increased compared to control (Figures S1D and S1E). *Ube3A* is also induced in response to environmental stimuli that trigger experience-dependent synaptic development (Figure 1C and Figure S1F). Mice in a cage containing novel objects to induce exploratory behavior exhibited increased *Ube3A* mRNA and protein expression compared to mice in a standard laboratory cage (Figure 1C and Figure S1F). These results demonstrate that *Ube3A* mRNA and protein levels are regulated by synaptic activity both in culture and in the intact brain. These findings raise the possibility that synaptic glutamate release during early life experiences activates *Ube3A* expression and that the absence of experience-dependent *Ube3A* induction may contribute to the neurological impairment in AS.

We investigated the mechanism by which neuronal activity triggers *Ube3A* induction. Analysis of *Ube3A* transcripts present in expressed sequence tag databases revealed three distinct mRNA transcripts that are likely transcribed from unique promoters. Of the *Ube3A* transcripts, those initiating from promoters 1 and 3 are induced by neuronal activity (Figure S1G), and their promoters contain binding sites for the activity-regulated transcription factor MEF2. These sites are conserved across phylogeny and lie within 2 kB of the putative transcriptional start sites of the two activity-regulated *Ube3A* transcripts (see below). The presence of potential MEF2-binding sites within *Ube3A* promoters was of interest because MEF2 is an activity-regulated transcription factor that controls synapse development and regulates genes implicated in ASDs (Flavell et al., 2006; Flavell et al., 2008; Morrow et al., 2008).

Chromatin immunoprecipitation experiments revealed that DNA fragments corresponding to *Ube3A* promoters 1 and 3 are enriched in anti-MEF2 immunoprecipitates (Figure 1D and data not shown). By contrast, there was no enrichment for DNA sequences surrounding *Ube3A* promoter 2 (Figure 1D). These data suggest that MEF2 may directly control the activity-dependent transcription of *Ube3A* from promoters 1 and 3.

The neuronal activity-dependent induction of *Ube3A* promoter 1- and 3-driven mRNA transcripts and Ube3A protein are significantly reduced in neurons infected with lentiviruses encoding short hairpin RNAs (shRNAs) targeting the *MEF2* family members *MEF2A* and *MEF2D* (Figures 1E and 1F). By contrast, the expression of *Ube3A* promoter 2-dependent mRNA transcripts, as well as *GAPDH* and *beta3-tubulin*, is unaffected by the presence of MEF2 shRNA (Figure 1E). These experiments indicate that in response to neuronal activity, *Ube3A* promoter 1- and 3-driven mRNA transcripts and Ube3A protein expression are induced by a MEF2-dependent mechanism.

Identification of Ube3A Substrates

Regulation of *Ube3A* mRNA expression by neuronal activity along with the association of *Ube3A* with AS led us to investigate the role of Ube3A in nervous system development. Point mutations within the *Ube3A* coding region have been associated with AS, nearly all of which abrogate its E3 ubiquitin ligase activity (Cooper et al., 2004), suggesting that the catalytic activity of Ube3A is important for nervous system development.

Although several Ube3A substrates have been identified in nonneuronal cells, the identification of substrates of E3 ubiquitin ligases has been challenging. To identify Ube3A substrates, we employed a transgenic mouse in which a hemagglutinin epitope tagged-version of ubiquitin (HA-ubiquitin) is knocked into the HPRT locus (Ryu et al., 2007). These mice express similar levels of free ubiquitin in their brains to those detected in the brains of wild-type mice (Figure 2A). In addition, in the HA-ubiquitin mice HA-ubiquitin appears to be efficiently incorporated into substrates (Figures 2A and 2B). We crossed HA-ubiquitin transgenic mice with wild-type or *Ube3A* knockout mice and immunoprecipitated HA-ubiquitinated proteins from brain lysates of these mice. We then compared ubiquitinated proteins in wild-type and *Ube3A* knockout mice using quantitative mass

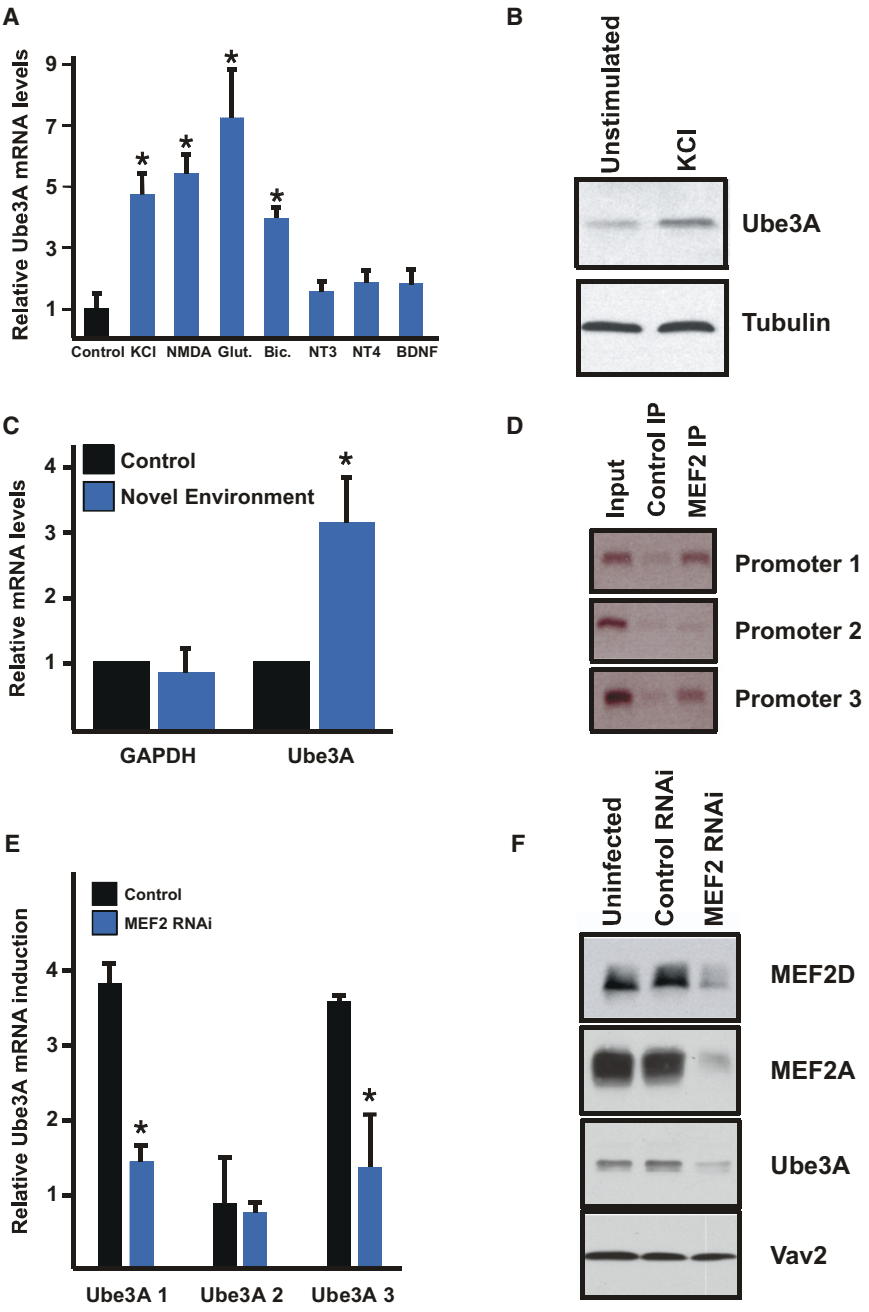

Figure 1. Regulation of Ube3A by Neuronal Activity

(A) qRT-PCR analysis of *Ube3A* mRNA extracted from hippocampal neurons at E18 + 10 days in vitro (DIV) stimulated for 5 hr with the indicated agent (Glut., glutamate; Bic., bicuculline). Data are presented as mean ± SEM from three independent experiments. * indicates statistical significance in pairwise comparison to control: $p < 0.01$ t test.

(B) Western blot analyses of Ube3A and beta-tubulin. Protein lysates were collected from E18 + 10 DIV hippocampal neurons after stimulation with 55 mM KCl for 7 hr. Three independent experiments were performed, and a representative western blot is shown.

(C) qRT-PCR examining *Ube3A* and *GAPDH* mRNA levels in hippocampi of mice placed in standard laboratory cages (control) or in cages with novel objects (novel environment). The expression of *Ube3A* and *GAPDH* is normalized to the expression of *beta-tubulin*, which serves as an internal standard. Data are presented as mean ± SEM from three independent experiments. * indicates statistical significance in pairwise comparison: $p < 0.05$ t test.

(D) Chromatin immunoprecipitation with control or anti-MEF2 antibodies. PCR amplification is performed on genomic regions corresponding to the promoter regions of the three *Ube3A* transcripts.

(E) qRT-PCR analysis of the three *Ube3A* transcripts in hippocampal neurons transduced with lentivirus expressing either control shRNA or shRNAs targeting MEF2A and MEF2D. Neurons were stimulated with 55 mM KCl for 6 hr before mRNA was harvested. Data are plotted as fold induction of stimulated cells over unstimulated cells. Data are presented as mean ± SEM from three independent experiments. * indicates statistical significance in pairwise comparison: $p < 0.01$ t test.

(F) Western blot analyses of MEF2D, MEF2A, Ube3A, and the loading control Vav2. Protein lysates were collected from hippocampal neurons at E18 + 10 DIV. Neurons were uninfected or transduced with lentivirus encoding a control shRNA or shRNA targeting MEF2A and MEF2D at E18 + 3 DIV. This experiment was performed three times independently, and a representative western blot is shown here.

See also Figure S1.

spectrometry. We reasoned that if a given protein were a substrate of Ube3A, then in the absence of Ube3A it would be less ubiquitinated and thus less efficiently precipitated with anti-HA antibodies. We therefore sought to identify HA-ubiquitinated proteins whose abundance was decreased in *Ube3A* knockout mice.

We identified the protein Sacsin as a candidate Ube3A substrate. We found peptides corresponding to ubiquitinated Sacsin in brain lysates of wild-type but not *Ube3A* knockout mice, suggesting that Sacsin might not be efficiently ubiquitinated in the absence of Ube3A (Figure 2C). Sacsin is of interest as it is mutated in Charelvoix-Saguenay spastic ataxia, a neurological disorder with similarities to AS (Engert et al., 2000). However, little is known about Sacsin's role in nervous system development and the large size of the Sacsin protein suggested it would be difficult to study. Nevertheless, we found that Sacsin has a 75 amino acid stretch that has similarity to a previously identified Ube3A substrate HHR23A (Figure 2D). This region of homology corresponds to a well-characterized region of HHR23A consisting of five amphipathic helices, suggesting that the corresponding region in Sacsin may have a similar structure (Kamionka and Feigon, 2004). As the specificity of ubiquitin ligases is most strongly determined by substrate binding, we hypothesized that this region of similarity between Sacsin and

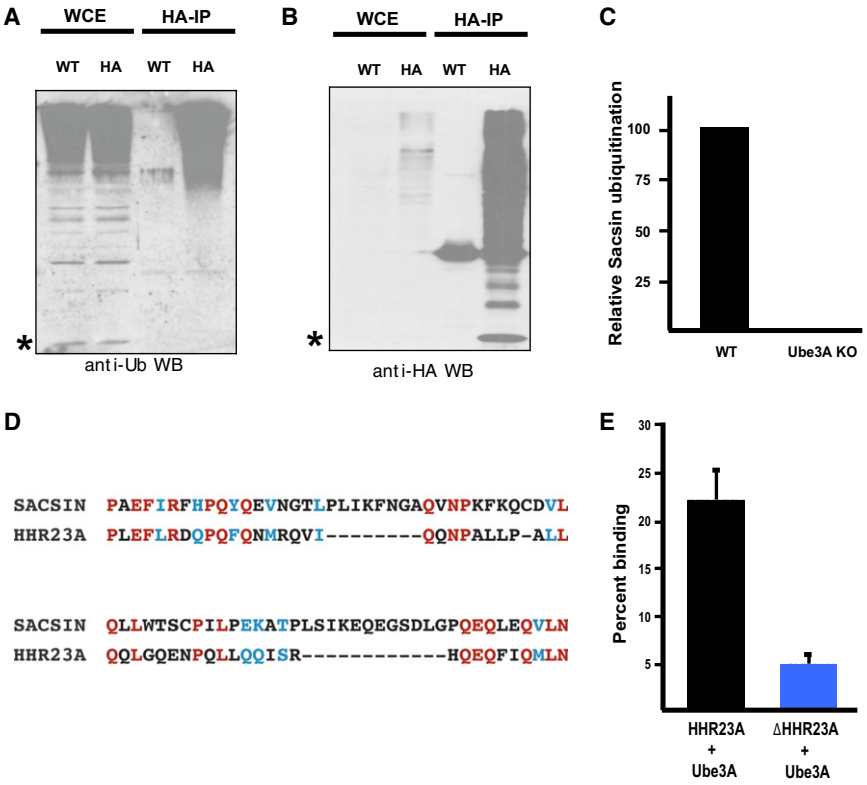

Figure 2. Identification of a Ube3A Binding Domain

(A) Analysis of ubiquitinated proteins in wild-type and HA-ubiquitin mice. Western blots using an anti-ubiquitin antibody were performed on cell lysates (WCE) or anti-HA immunoprecipitates from hippocampal mouse brain lysates prepared from wild-type (WT) or HA-ubiquitin transgenic (HA) mice. * indicates the presence of free ubiquitin.

(B) Analysis of ubiquitinated proteins in wild-type and HA-ubiquitin mice. Western blots using an anti-HA antibody were performed on cell lysates (WCE) or anti-HA immunoprecipitations from hippocampal mouse brain lysates from wild-type (WT) or HA-ubiquitin transgenic (HA) mice. * indicates the presence of free ubiquitin.

(C) Quantification of the relative abundance of ubiquitinated Sacsin in the brain of wild-type and *Ube3A* knockout mice. No peptides were detected corresponding to ubiquitinated Sacsin in *Ube3A* knockout mice.

(D) Sequence alignment of human Sacsin (amino acids 3660–3735) and human HHR23A (amino acids 231–285). Identical residues are in red and similar residues are in blue.

(E) Quantitative analysis of in vitro binding experiments using recombinant HHR23A, a version of HHR23A lacking the Ube3A binding domain (ΔHHR23A), and GST-Ub3A after precipitation with glutathione-Sepharose beads. Western blotting was performed using an anti-HHR23A antibody. Data are presented as mean ± SEM from three independent experiments.

HHR23A might serve as a Ube3A binding domain (UBD) that might be present in other Ube3A targets.

To test this hypothesis, we generated a mutant form of HHR23A (ΔHHR23A) that lacks the UBD and assessed its ability to interact with, and be ubiquitinated by Ube3A. While wild-type HHR23A efficiently interacts with Ube3A, mutation of the UBD in HHR23A blocks this interaction (Figure 2E). Likewise, this domain is required for Ube3A to ubiquitinate HHR23A (data not shown). These results suggest the existence of a motif on Ube3A substrates that mediates binding to Ube3A.

A search of mammalian genomes for proteins that contain the UBD identified proteins including the synaptic protein Arc and the RhoGEF ephexin 5 as potential Ube3A substrates (Figure 3A) (S.S. Margolis and M.E.G., unpublished data). We focused our attention on Arc as Arc regulates the trafficking of alpha-amino-3-hydroxy-5-methyl-4-isoxazole-propionate (AMPA) type of glutamate receptors at synapses (Chowdhury et al., 2006; Rial Verde et al., 2006; Shepherd et al., 2006). If Arc is a substrate of Ube3A, such a finding could potentially begin to explain Ube3A's role in synaptic function. Furthermore, like *Ube3A*, Arc transcription is regulated by neuronal activity through the action of MEF2 family transcription factors (Flavell et al., 2006), suggesting that these two proteins might function together in response to synaptic activation.

To assess whether Arc is a Ube3A substrate, we asked whether Arc and Ube3A interact. Purified Arc binds Ube3A in a manner that is dependent upon the UBD within Arc (Figures 3B and 3C). Coimmunoprecipitation experiments using mouse brain extracts confirmed that Arc and Ube3A also interact in the intact brain (Figure S2A). We then performed in vitro ubiquitination assays using purified recombinant proteins. Ube3A ubiquitinated Arc in vitro but did not ubiquitinate the control proteins p53 or MeCP2 (Scheffner et al., 1993) (Figure 3D and data not shown). A catalytically inactive form of Ube3A (Ube3A C833A) was incapable of catalyzing the ubiquitination of Arc (Kumar et al., 1999) (data not shown and see below).

To test whether Ube3A promotes the ubiquitination of Arc within cells, we transfected HEK293T cells with Arc and either Ube3A C833A or wild-type Ube3A. Coexpression of wild-type Ube3A, but not Ube3A C833A, led to a decrease in the level of Arc (Figure 3E). Incubation of transfected HEK293T cells with the proteasome inhibitor MG132 blocked Ube3A-mediated degradation of Arc, suggesting that Ube3A degrades Arc via the ubiquitin proteasome (Figure S2B). The ubiquitination of Arc by Ube3A was confirmed by mass spectrometry (Figures S2C and S2D).

We next compared Arc expression in the brains of wild-type and *Ube3A* knockout mice. As the expression of both Ube3A and Arc is enhanced by neuronal activity, we exposed the mice to kainic acid or an enriched environment to boost the levels of Ube3A and Arc protein. Under these conditions, we detect higher levels of Arc protein in *Ube3A* knockout mice than in wild-type controls (Figures 3F–3H). These findings suggest that Ube3A ubiquitination of Arc in the wild-type brain contributes to Arc degradation. In contrast to Arc, the activity-dependent phosphorylation of the transcriptional regulator MeCP2 and the

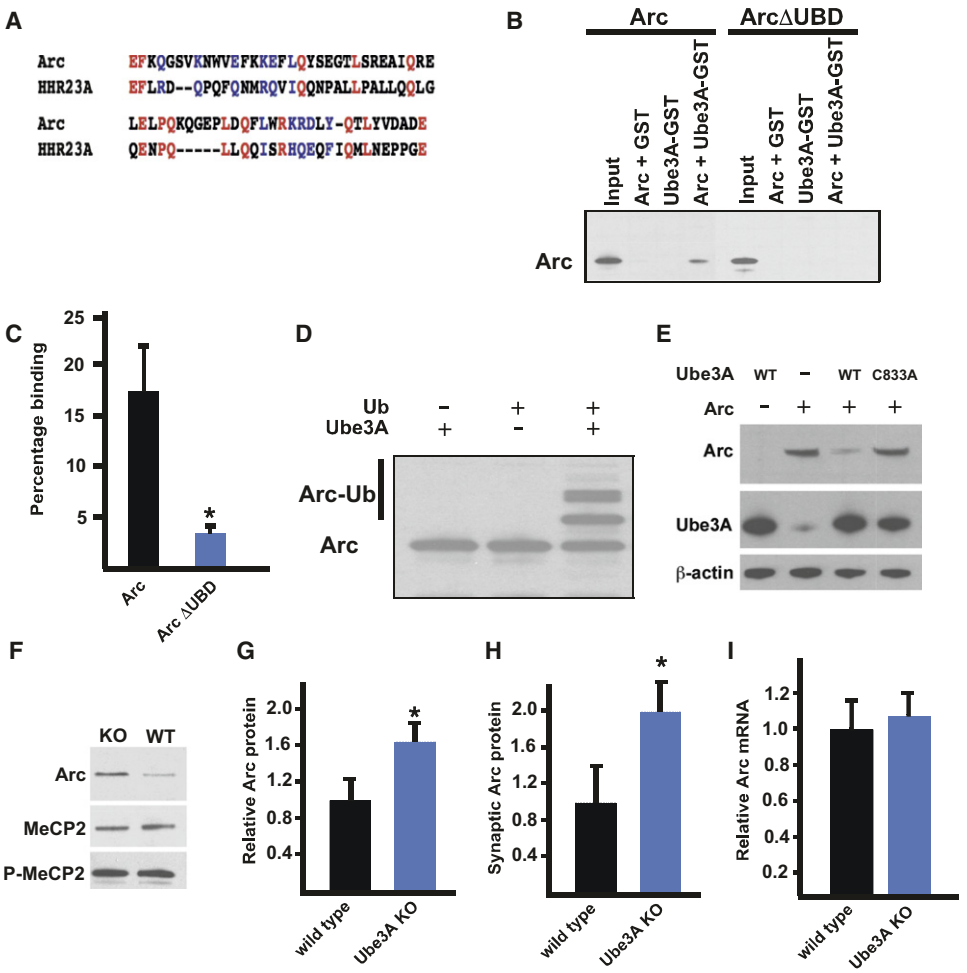

Figure 3. Arc Is a Ube3A Substrate

(A) Sequence alignment of Arc (amino acids 255–318) and HHR23A (amino acids 233–290). Identical residues are in red and similar residues are in blue. We would like to note that as the UBD may represent a sequence that encodes a particular protein folding structure, a strict one-to-one map of specific residues is not observed. Dashed lines indicate a gap in sequence.

(B) In vitro binding experiments using recombinant Arc, ArcΔUBD, and GST-tagged Ube3A, precipitated with glutathione Sepharose beads and western blotted with an anti-Arc antibody.

(C) Quantitative analysis of in vitro binding experiments using recombinant Arc, or ArcΔUBD, and Ube3A. Western blotting was performed with an anti-Arc antibody. Percentage binding refers to the percent of Arc bound to Ube3A relative to the input. Data are presented as mean ± SEM from three independent experiments. * indicates statistical significance $p < 0.01$, t test.

(D) In vitro ubiquitination assay of Arc in the presence of Ubiquitin (Ub) and/or Ube3A.

(E) Western blot analysis using anti-Arc, anti-Ube3A, or anti-actin antibodies on lysates from HEK293T cells transfected with the indicated constructs.

(F) Western blot analysis of protein lysates prepared from the hippocampi of wild-type and *Ube3A* knockout mice which had been injected with kainic acid. Western blots performed with anti-MeCP2, anti-phospho-MeCP2, and anti-Arc antibodies as indicated. Three individual experiments representing at least five animals per genotype were performed, and a representative example is shown.

(G) Quantification of Arc protein by western blot analysis of protein lysates prepared from hippocampi of wild-type and *Ube3A* knockout mice which had been exposed to an enriched environment. Data represent mean ± SEM from four animals of each genotype. * denotes significance in pairwise comparison to control: $p < 0.01$ t test.

(H) Quantification of Arc protein by western blot analysis of protein lysates prepared from synaptosomes isolated from hippocampi of wild-type and *Ube3A* knockout mice that had been injected with kainic acid. Data represent mean ± SEM from three animals of each genotype. * denotes significance in pairwise comparison to control: $p < 0.05$ t test.

(I) Real-time quantitative PCR analysis of *Arc* mRNA extracted from wild-type and *Ube3A* knockout mice seized with kainic acid used in (F). Data are presented as mean ± SEM from three independent experiments.

See also Figure S2.

induction of the activity-regulated transcription factor NPAS4 are similar in wild-type and *Ube3A* knockout brains, suggesting that the increase in Arc in *Ube3A* knockout mouse brain is not the result of an overall increase in the activity-dependent gene response (Figure 3F and data not shown) (Zhou et al., 2006; Lin et al., 2008). Furthermore, *Arc* mRNA levels are similar in the

brains of wild-type and *Ube3A* knockout mice, indicating that the increase in the level of Arc protein detected in *Ube3A* knockout neurons is likely due to a defect in Ube3A-mediated degradation of Arc (Figure 3I). Given that Arc is ubiquitinated by Ube3A in vitro and in intact cells and that the level of Arc protein is significantly higher in *Ube3A* knockout mice, we conclude that Arc is a Ube3A substrate and that the decreased ubiquitination of Arc in *Ube3A* knockout mice results in increased levels of Arc in the brains of these animals.

Regulation of AMPA Receptor Expression and Function by Ube3A

Arc regulates the surface expression of AMPA receptors (AMPARs), mediators of fast excitatory neurotransmission in the CNS. Reduction of Arc expression leads to an increase in the surface expression of AMPARs, whereas increasing Arc levels decreases the plasma membrane expression of AMPARs (Chowdhury et al., 2006; Rial Verde et al., 2006; Shepherd et al., 2006). As Arc levels are elevated in the absence of Ube3A, it is possible that there is a concomitant decrease in the expression of AMPARs on the plasma membrane. Such a finding would suggest a mechanism for the cognitive dysfunction observed in individuals with AS.

We asked whether reduction of Ube3A expression decreases the plasma membrane expression of AMPARs. We decreased Ube3A expression by transfecting neurons with shRNAs that target Ube3A expression and then assessed the surface expression of AMPARs (Figures S3A and S3B). We focused on the GluR1 subunit of the AMPA receptor, as GluR1 insertion into the plasma membrane is regulated by neuronal activity and by Arc (Newpher and Ehlers, 2008; Kessels and Malinow, 2009; Rial Verde et al., 2006; Shepherd et al., 2006). To examine GluR1 expression at the plasma membrane of neurons, we stained hippocampal neurons with anti-GluR1 antibodies under nonpermeabilizing conditions and quantified the number of GluR1 puncta expressed on the cell surface. Expression of either of two shRNAs targeting Ube3A results in a reduction in the levels of GluR1 expressed at the plasma membrane that is rescued by coexpression of an RNA interference (RNAi)-resistant form of Ube3A (Figure 4A and Figure S3C). This decrease in surface GluR1 was not due to a change in the expression of AMPARs, as wild-type and Ube3A-deficient cells expressed similar levels of GluR1 and GluR2 subunits (data not shown). Furthermore, the plasma membrane expression of NR1 subunits of the NMDA receptor was unaltered in Ube3A-deficient cells (Figure 4B).

As AMPA receptors are trafficked in and out of synapses, we examined the effect of Ube3A knockdown on surface postsynaptic AMPA levels, quantifying the number of GluR1 cell surface puncta that colocalize with the postsynaptic scaffolding protein PSD95. We find that shRNAs targeting Ube3A cause a reduction in the number of GluR1 puncta colocalizing with PSD95, indicating that Ube3A regulates recruitment of AMPA receptors to the postsynaptic region (Figure 4C).

We asked whether AMPAR endocytosis is enhanced in the absence of Ube3A. We used GluR1-specific antibodies to label surface AMPARs on neurons transfected with shRNAs targeted to Ube3A. After membrane depolarization to induce the endocytosis of synaptic AMPARs, anti-GluR1 antibodies bound to the remaining surface GluR1 subunits were removed by acid stripping (Man et al., 2007). Subsequent permeabilization of the cells and staining with fluorescent secondary antibodies to detect the internalized component of GluR1 revealed increased levels of endocytosed GluR1 in Ube3A shRNA-expressing cells compared to control shRNA-transfected neurons (Figure 4D). Thus, the decreased expression of AMPARs in the plasma membrane of synapses of Ube3A-deficient cells is due, at least in part, to an increase in AMPAR endocytosis.

To investigate whether increased AMPAR endocytosis affects AMPAR function at synapses, we recorded miniature excitatory postsynaptic currents (mEPSCs) in neurons expressing Ube3A-directed shRNAs. Compared to control shRNAs, the transfection of Ube3A shRNAs results in a significant decrease in mEPSC frequency with no change in mEPSC amplitude (Figures 4E–4G). This decrease in mEPSC frequency could be rescued by coexpression of an RNAi-resistant form of Ube3A. As mEPSC frequency is a measure of AMPAR-mediated synaptic transmission, this observation suggests that AMPAR function is altered at synapses of Ube3A deficient neurons.

The observation that when Ube3A expression is knocked down there is a reduction in mEPSC frequency with no change in mEPSC amplitude could be explained by any of three possibilities: (1) a reduction in the number of synapses formed on the Ube3A deficient neuron, (2) reduced presynaptic probability of neurotransmitter release from neurons that synapse onto Ube3A deficient neurons, or (3) a subset of synapses that form on Ube3A-deficient neurons could lack AMPA receptors and thus would be "silent synapses," not readily detected by mEPSC recordings. To distinguish between these possibilities, we determined whether there are fewer synapses formed when Ube3A is knocked down. At the time point of analysis where we detect reduced mEPSC frequency, we observe no significant change in dendritic spine density or the number of synapses that form on Ube3A shRNA-expressing neurons (Figures S3D and S3E). These findings, and the absence of any detectable change in the formation of inhibitory synapses, neuronal morphology, or cell survival when Ube3A expression is knocked down (data not shown), suggest that the decrease in mEPSC frequency does not reflect a decrease in the number of synaptic connections formed on Ube3A-deficient neurons.

Although we cannot rule out the possibility that a decrease in Ube3A expression in the postsynaptic neuron reduces the presynaptic probability of release, we favor the hypothesis that the loss of Ube3A leads to the elimination of AMPAR expression from a subset of synapses for a number of reasons, including the following: (1) loss of Ube3A function results in an increase in the levels of Arc, a protein whose expression has been shown to promote the endocytosis of AMPAR, (2) in the absence of Ube3A, we observe fewer GluR1 puncta that colocalize with PSD95, suggesting that when the level of Ube3A protein is reduced there are synapses that may not express AMPARs, and (3) there is a reduction in the ratio of AMPA/NMDA receptor-mediated transmission in *Ube3A* knockout neurons (see below), consistent with the idea that some synapses that form on Ube3A-deficient neurons lack AMPARs.

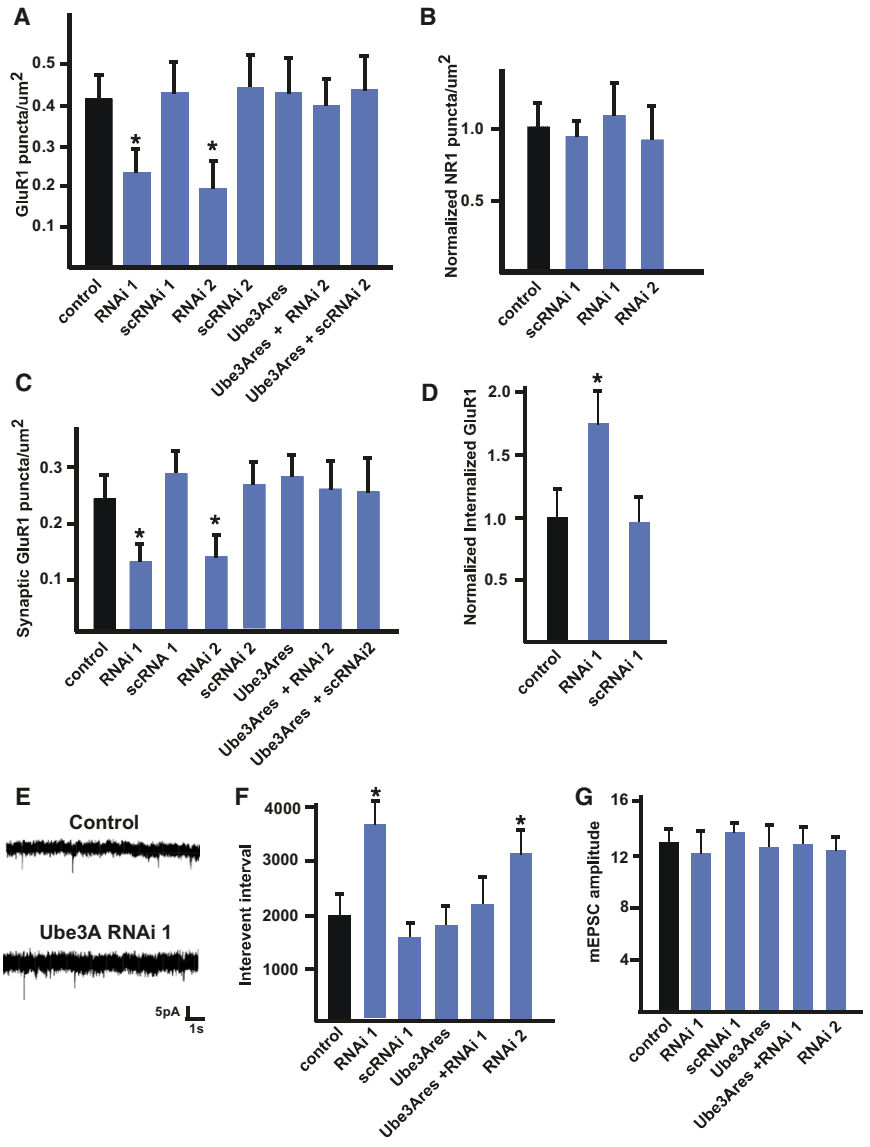

Figure 4. Ube3A Regulates AMPAR Function

(A) Quantification of plasma membrane expression of AMPARs on E18 + 14 DIV hippocampal neurons transfected at 10 DIV with GFP and vector control, either of two shRNAs targeting Ube3A (RNAi 1 or 2), scrambled control shRNA (scRNAi 1 or 2), a form of Ube3A that is resistant to Ube3A shRNA (Ube3Ares), or Ube3A shRNA and Ube3A that is RNAi resistant (Ube3Ares + RNAi 2). At least 35 neurons were imaged for each condition. Data are presented as mean ± SEM from three independent experiments. * indicates statistical significance $p < 0.05$, ANOVA with a Bonferroni correction for multiple comparisons.

(B) Quantification of plasma membrane expression of NMDA receptors on E18 + 14 DIV hippocampal neurons transfected at 10 DIV with GFP and vector control, either of two shRNAs targeting Ube3A (RNAi 1 or 2), or a scrambled control shRNA (scRNAi 1). At least 20 neurons were imaged for each condition, and data are presented as mean ± SEM from three independent experiments.

(C) Same as in (A) except only GluR1 puncta that colocalize with PSD95 are counted. At least 29 neurons were imaged for each condition, and data are presented as mean ± SEM from three independent experiments. * indicates statistical significance $p < 0.05$, ANOVA with a Bonferroni correction for multiple comparisons.

(D) Quantification of internalized GluR1 receptors from E18 + 14 DIV hippocampal neurons transfected at 10 DIV with GFP plus vector, Ube3a shRNA, or control scrambled shRNA. Data are presented as mean ± SEM from three independent experiments. * indicates statistical significance $p < 0.05$, ANOVA with a Bonferroni correction for multiple comparisons.

(E) Representative mEPSC traces of control transfected (top) or Ube3A RNAi transfected neurons (bottom) used for analysis in (F) and (G).

(F) Quantification of mEPSC interevent interval (the time between mEPSC events and thus inversely proportional to mEPSC frequency) from E18 + 14 DIV hippocampal neurons transfected as in (A). Data are presented as mean ± SEM from three independent experiments. * indicates statistical significance $p < 0.01$, t test.

(G) Quantification of mEPSC amplitude from E18 + 14 DIV hippocampal neurons transfected as in (A). Data are presented as mean ± SEM from three independent experiments.

See also Figure S3.

Arc Mediates the Effect of Ube3A on AMPAR Trafficking

We asked whether Ube3A enhances AMPAR endocytosis by ubiquitinating and degrading Arc. If the enhanced AMPAR endocytosis observed after Ube3A knockdown is mediated by the dysregulation of the ubiquitination of Arc, we would make the following predictions: (1) Ube3A's ubiquitin ligase activity would be required for its effect on AMPAR endocytosis, (2) overexpression of Arc would phenocopy the loss of Ube3A and reduce AMPAR plasma membrane expression, and (3) in Ube3A-deficient cells, restoring Arc expression to the level seen in wild-type neurons should rescue the decrease in GluR1 surface expression observed in the absence of Ube3A.

To test these predictions, we examined whether the ubiquitin ligase activity of Ube3A is required for Ube3A to promote AMPAR expression at synapses. We generated a Ube3A mutant in which the cysteine residue within the active site of the Ube3A ligase is mutated to alanine (Ube3A C833A), reasoning that when overexpressed this mutant should act in a dominant interfering manner to block the ability of endogenous Ube3A to ubiquitinate its substrates. We found this to be true as overexpression of Ube3A C833A blocks the ability of wild-type Ube3A to ubiquitinate and degrade its substrates (Figures 5A–5C). To determine whether Ube3A's ubiquitin ligase activity is required for Ube3A to enhance AMPAR expression at synapses, we

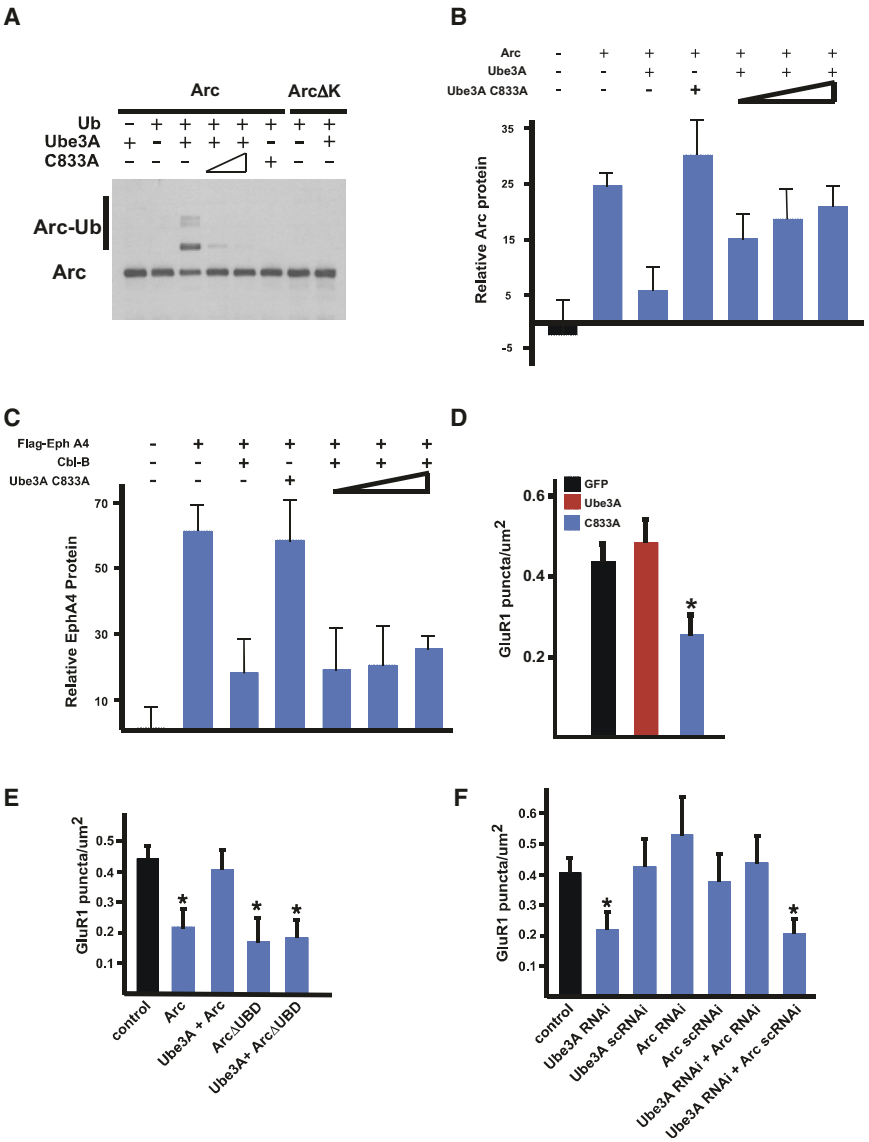

Figure 5. Ube3A-Mediated Degradation of Arc Affects AMPAR Cell Surface Expression

(A) In vitro ubiquitination assay of Arc or a version of Arc in which all lysine residues are mutated to arginine (ArcΔK) in the presence of Ubiquitin (Ub), Ube3A, or Ube3A C833A (C833A). Western blotting analysis was performed with an anti-Arc antibody.

(B) Quantitative western blot analysis of protein lysates from HEK293T cells transfected with the indicated constructs. Western blots were performed with an anti-Arc antibody, and the signals were normalized to an actin loading control.

(C) Quantitative western blot analysis of protein lysates from HEK293T cells transfected with the indicated constructs. Western blots were performed using an anti-Flag antibody to detect EphA4, and the resultant values were normalized to an actin loading control. As previously reported, Cbl-B promotes the degradation of EphA4 (Sharfe et al., 2003). Cbl-B-mediated degradation of EphA4 is not inhibited by Ube3A C833A, even though Ube3A and Cbl-B can employ the same E2 conjugating enzyme when ubiquitinating substrates.

(D) Quantification of surface AMPAR expression for E18 + 17 DIV hippocampal neurons transfected with GFP and vector control, Ube3A, or Ube3A C833A plasmids. At least 30 neurons were imaged for each condition, and data are presented as mean ± SEM from three independent experiments. * indicates statistical significance $p < 0.05$, ANOVA, with Bonferroni correction for multiple comparison.

(E) Quantification of surface AMPA receptor expression on E18 + 14 DIV hippocampal neurons transfected at 10 DIV with vector control, Arc, Ube3A + Arc, ArcΔUBD, or ArcΔUBD + Ube3A. Data are presented as mean ± SEM from three independent experiments. * denotes statistical significance $p < 0.05$, ANOVA, with Bonferroni correction for multiple comparison.

(F) Quantification of surface AMPAR expression on hippocampal neurons transfected with vector control, Ube3A RNAi, Ube3A scrambled RNAi, Arc RNAi, Arc scrambled RNAi, Ube3A RNAi and scrambled control Arc RNAi, or Ube3A RNAi and Arc RNAi. Data are presented as mean ± SEM from three independent experiments. * denotes statistical significance $p < 0.05$, ANOVA, with Bonferroni correction for multiple comparison.

See also Figures S4 and S5.

transfected neurons with wild-type Ube3A or Ube3A C833A. Overexpression of Ube3A C833A but not wild-type Ube3A causes a significant reduction in the number of AMPARs present on the cell surface, suggesting that Ube3A ubiquitin ligase activity is critical to the ability of Ube3A to promote expression of AMPARs at synapses (Figure 5D and Figure S4A).

We asked whether the overexpression of Arc phenocopies the loss of Ube3A and reduces AMPAR expression. As previously reported, the overexpression of Arc results in a decrease in the plasma membrane expression of GluR1 (Chowdhury et al., 2006; Rial Verde et al., 2006; Shepherd et al., 2006) (Figure 5E). Coexpression of Ube3A with wild-type Arc attenuates the ability of Arc to promote the endocytosis of GluR1. When a version of Arc lacking the UBD (ArcΔUBD) was overexpressed in neurons, this form of Arc still promoted the endocytosis of GluR1 but the co-expression of Ube3A did not reverse this effect (Figure 5E). This suggests that Ube3A's ability to reduce the endocytosis of AMPARs is due to Ube3A-mediated degradation of Arc.

To further investigate whether the ability of Ube3A to promote the expression of AMPARs at synapses is due to Ube3A-dependent Arc ubiquitination and degradation, neurons were transfected with shRNAs targeting Ube3A to reduce Ube3A expression and/or shRNA directed against Arc to decrease Arc expression and the effect on AMPAR cell surface expression assessed. As described above, the expression of shRNAs

targeting Ube3A in neurons led to a reduction in the number of AMPARs at the neuronal cell surface (Figure 5F). Introduction of shRNAs directed against Arc, but not control shRNAs, significantly reduced Arc expression in HEK293T cells (Figure S4B) and when transfected into neurons caused a small but statistically insignificant increase in surface AMPAR expression (Figure 5F). The failure of Arc shRNAs when transfected alone to affect AMPAR surface expression likely reflects the fact that given the low level of neuronal activity in these cultures Arc levels are also quite low and only minimally affect AMPAR surface expression. Consistent with this possibility, in older cultures the expression of Arc shRNAs results in an increase in AMPAR plasma membrane expression (Figure S4C). The lack of significant Arc expression in younger neuronal cultures may also explain why we find that overexpression of Ube3A does not significantly affect the plasma membrane expression of AMPARs in younger neuronal cultures. Expression of shRNAs against Ube3A together with an shRNA directed against Arc blocked the ability of Ube3A shRNA to suppress AMPAR expression at synapses (Figure 5F and Figure S5). These findings suggest that Ube3A promotes the expression of AMPARs at the plasma membrane of synapses by ubiquitinating and degrading Arc and that in the absence of Ube3A there is an excess of Arc protein, resulting in increased endocytosis of AMPARs.

Analysis of AMPAR Function in *Ube3A* Knockout Mice

These findings suggest that in AS, the absence of Ube3A activity may lead to an increase in Arc expression, thereby resulting in a reduction in the expression of AMPARs at synapses. To investigate this, we examined AMPAR expression and function at the synapses of *Ube3A* knockout mice that display features of AS (Jiang et al., 1998). We cultured neurons from *Ube3A* knockout or wild-type mice and assessed the expression of AMPARs. *Ube3A* knockout neurons had reduced GluR1 expression at the plasma membrane of synapses when compared to wild-type neurons (Figure 6A). This effect appears to be specific to AMPARs as we observe no change in the surface expression of NMDARs (Figure 6B). Expression of shRNAs targeting Arc in *Ube3A* knockout neurons restores the expression of GluR1 surface expression in *Ube3A* knockout neurons (Figure 6C). These experiments suggest that the excessive internalization of AMPARs in *Ube3A* knockout neurons is likely a result of a failure to ubiquitinate and degrade Arc.

To determine whether GluR1 expression at synapses is dysregulated in *Ube3A* knockout neurons in the context of an intact neuronal circuit, we employed array tomography, a technique in which ultra-thin sections of brain tissue are stained, imaged, and synapses visualized as a 3D reconstruction (Micheva and Smith, 2007). We performed array tomography using anti-GluR1 antibodies to visualize AMPARs and anti-SV2 antibodies to mark presynaptic sites. The density of GluR1 puncta closely apposed to an SV2 puncta is decreased in *Ube3A* knockout mice (Figure 6D and Figure S6). The density of SV2 puncta remained constant between the two genotypes, suggesting that the decrease in GluR1 synaptic localization in *Ube3A* knockout sections is not a result of fewer available presynaptic sites and instead reflects a decrease in GluR1 expression at synapses. In contrast, we found that the number of NR1 puncta associated with SV2 puncta was similar at the synapses in the hippocampi of wild-type and *Ube3A* knockout mice, suggesting that the expression of AMPARs is selectively decreased in the brains of *Ube3A* knockout mice (Figures 6E and 6F and Figure S6). This reduction in AMPAR expression at the synapses of *Ube3A* knockout mice is not a result of decreased overall expression of GluR1 as wild-type and *Ube3A* knockout mice express similar levels of GluR1 and NR1 in their hippocampi (Figure 6G).

To determine whether the decreased expression of AMPARs at the synapses of *Ube3A* knockout mice results in a functional decrease in synaptic transmission, whole-cell recordings were made from CA1 hippocampal pyramidal neurons. We observe a significant decrease in the ratio of AMPA to NMDA receptor-mediated currents in *Ube3A* knockouts compared to wild-type mice (Figures 7A and 7B). While this decrease in AMPA/NMDA current receptor ratio could reflect either a decrease in AMPAR or an increase in NMDAR currents, our findings that in *Ube3A* knockout mice there is a decrease in AMPAR expression at synapses but no change in NMDAR expression suggests that the decrease in AMPA/NMDA current ratio is most likely due to a decrease in AMPAR-mediated currents in *Ube3A* knockout mice.

As an independent means of assessing the effect of disrupting Ube3A on AMPAR function, we recorded mEPSCs from wild-type and *Ube3A* knockout hippocampal pyramidal neurons in acute slice preparations. We observe a reduction in the frequency of mEPSCs with no corresponding change in mIPSC frequency or amplitude in *Ube3A* knockout neurons compared to wild-type neurons (Figures 7C–7E and Figure S7). This observation supports the conclusion that AMPAR expression and function at synapses are significantly decreased in *Ube3A* knockout neurons.

DISCUSSION

Although it has been appreciated for more than a decade that mutation of *Ube3A* results in AS, remarkably little is understood about the role of Ube3A in nervous system development and function or why mutation of *Ube3A* results in the cognitive impairment underlying AS. This lack of insight has hampered the development of therapeutic strategies for treating AS, and as a result there are currently no effective treatments for this disorder. In this study, we demonstrate that in the absence of synaptic activation, Ube3A and Arc are expressed at low levels. However, in response to glutamate release at excitatory synapses, Arc is induced with relatively rapid kinetics (Flavell et al., 2006) and endocytoses AMPAR from the plasma membrane. This induction of Arc is likely important for limiting the level of neuronal excitation since Arc-mediated endocytosis of AMPARs dampens neuronal excitability. However, the level of Arc expression must be effectively regulated for synapses to function appropriately. We find that *Ube3A* transcription is induced postsynaptically upon glutamate release at synapses with delayed kinetics relative to *Arc* and that Ube3A then functions to control the level of Arc protein expression by ubiquitinating and degrading Arc. In this way, Ube3A tempers the Arc-mediated internalization of AMPARs. The absence of Ube3A activity in *Ube3A* knockout mice results in increased

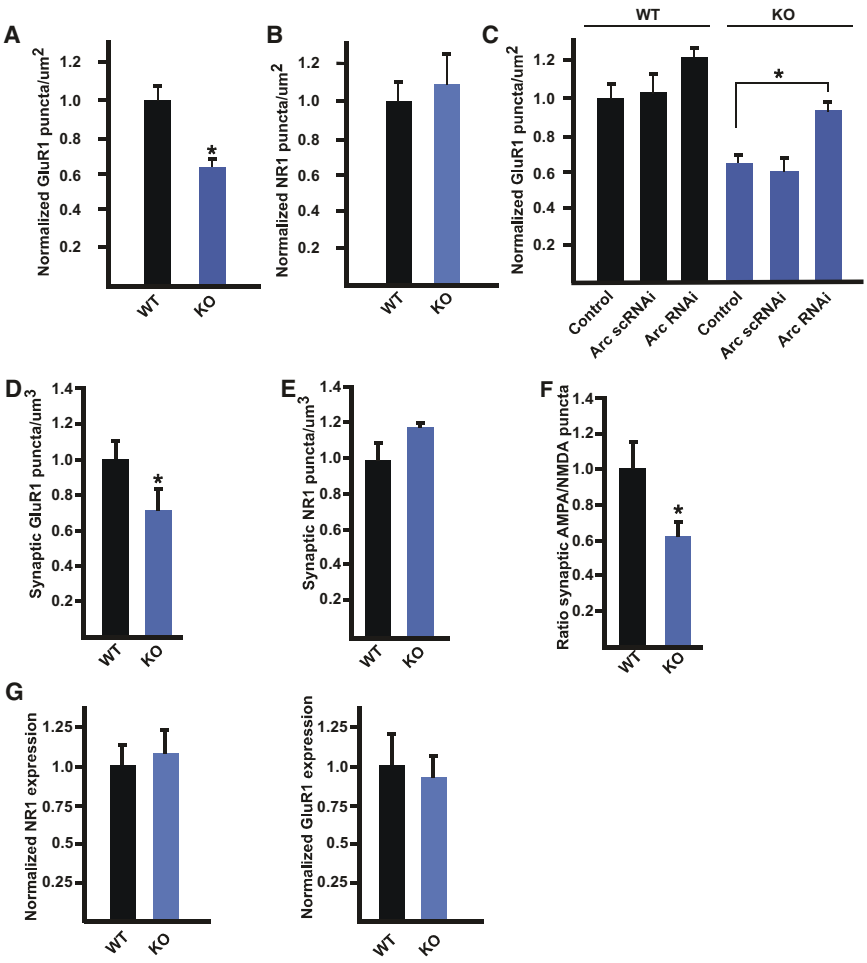

Figure 6. *Ube3A* Knockout Mice Have Fewer Synaptically Expressed AMPARs

(A) Quantification of plasma membrane expression of AMPARs on P2 + 12 DIV hippocampal neurons isolated from wild-type (WT) and *Ube3A* knockout (KO) animals transfected at 8 DIV with GFP. At least 40 neurons were imaged for each condition, and data are normalized to wild-type and presented as mean ± SEM from three independent experiments. * indicates statistical significance $p < 0.01$, t test.

(B) Quantification of plasma membrane expression of NMDA receptors on P2 + 12 DIV hippocampal neurons isolated from wild-type (WT) and *Ube3A* knockout (KO) animals transfected at 8 DIV with GFP. At least 24 neurons were imaged for each condition, and data are normalized to wild-type and presented as mean ± SEM from three independent experiments.

(C) Quantification of plasma membrane expression of AMPA receptors on P2 + 12 DIV hippocampal neurons isolated from wild-type (WT) and *Ube3A* knockout (KO) animals transfected at 8 DIV with GFP and either vector control, scrambled control shRNAs, or shRNAs targeting Arc. At least 28 neurons were imaged for each condition, and data are normalized to wild-type transfected with control and presented as mean ± SEM from three independent experiments. * indicates statistical significance $p < 0.01$, ANOVA, with Bonferroni correction for multiple comparisons.

(D) Quantification of the number of colocalized GluR1 and SV2 puncta in wild-type and *Ube3A* knockout hippocampi. Data are presented as mean ± SEM from three independent animals for each genotype. * indicates statistical significance $p < 0.01$, t test.

(E) Quantification of the number of colocalized NR1 and SV2 puncta in wild-type and *Ube3A* knockout hippocampi. Data are presented as mean ± SEM from three independent animals for each genotype. $p > 0.05$, t test.

(F) Analysis of the ratio of the density of GluR1 puncta that colocalize with SV2 to the density of NR1 puncta that colocalize with SV2 obtained from (D) and (E). * indicates statistical significance $p < 0.01$, t test.

(G) Quantitative western blot analysis of protein lysates prepared from the hippocampi of P21 wild-type and *Ube3A* knockout mice using anti-NR1 (left) and anti-GluR1 (right) antibodies. Band intensity was normalized to the intensity of actin to control for differences in protein concentration. Data are presented as mean ± SEM from three independent experiments.

See also Figure S6.

levels of Arc, and excessive internalization of AMPARs, leading to fewer synapses that express AMPARs at the plasma membrane and to defects in synaptic transmission.

Consistent with these observations, a recent study has demonstrated that Ube3A plays a role in experience-dependent synaptic plasticity (Yashiro et al., 2009). Although Ube3A is not required for the initial sensory-independent stages of synapse development, Ube3A is necessary for sensory experience-driven maturation of excitatory circuits, as *Ube3A* knockout mice have deficits in LTP, LTD, and decreased mEPSCs in visual cortex. The observation that Ube3A plays a role in experience-driven synaptic plasticity may be explained by our finding that both *Arc* and *Ube3A* transcription are induced by sensory experience and that in response to neuronal activity in the absence of Ube3A, there is excessive accumulation of Arc and increased internalization of AMPARs. As AMPARs play a central role in neurotransmission and information processing, this defect in AMPAR expression and function in the absence of Ube3A is likely to explain, at least in part, the deficits in synaptic plasticity observed in the absence of Ube3A.

Our findings suggest that AS may be caused by the disruption of a crucial step in experience-dependent synaptic development and provide evidence that the neuronal activity-regulated gene program plays a key role in human cognitive development. Further support for this hypothesis comes from the observation that mutation of another activity-regulated MEF2 target gene, *Slc9A6*, results in phenotypes that mimic AS (Gilfillan et al., 2008). Recent studies have shown that additional components of the activity-regulated gene program including *L-VSCC*, *RSK2*, *MeCP2*, *CBP*, *PDCH10*, and *DIA1* are mutated in human disorders, particularly epilepsy and ASDs (reviewed in Greer and Greenberg, 2008). These findings suggest that further

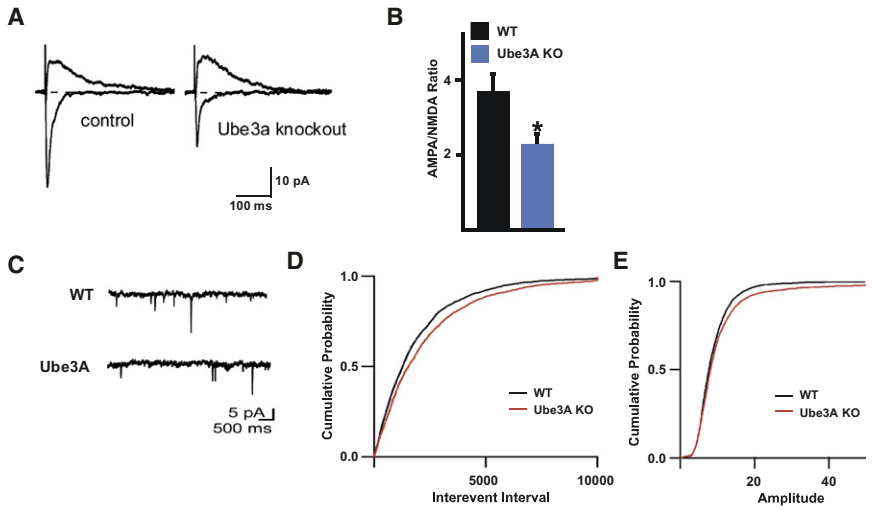

Figure 7. Analysis of Synaptic Function in the Hippocampi of *Ube3A* Knockout Mice

(A) Representative traces of currents evoked while holding the neuron at −70 or +40 mV to measure AMPAR- or NMDAR-mediated currents, respectively. Examples are shown from a control (left) and *Ube3A* knockout (right) neuron. Currents are scaled by the current amplitude measured between 50 and 70 ms after the peak of the evoked current at +40 mV to highlight the relative changes in AMPAR-mediated current.

(B) A summary histogram of AMPA/NMDA receptor-mediated current ratios presented as the geometric mean ± SEM. At least 15 cells were analyzed per condition. * $p < 0.05$ by students t test of the geometric means for each neuron.

(C) Representative mEPSC traces of hippocampal neurons from wild-type (top) and *Ube3A* knockout (bottom) slices.

(D) Quantification of mEPSC frequency from wild-type (black line) and *Ube3A* knockout (red line) mice. Data are presented as cumulative probability plots of interevent intervals and represent recordings from at least 14 neurons from at least three independent animals of each genotype. A significant difference was observed between wild-type and *Ube3A* knockout mice, $p < 0.01$ by Kolmogorov-Smirnov (KS) test.

(E) Quantification of mEPSC amplitude from wild-type (black line) and *Ube3A* knockout (red line) mice. Data are presented as cumulative probability plots and represent recordings from at least 14 neurons from at least three independent animals of each genotype. No statistically significant difference was observed between wild-type and *Ube3A* knockout mice by KS test.

See also Figure S7.

investigation into the regulation and function of Ube3A, and the activity-dependent gene program in general, will provide new insight into the mechanisms controlling human cognitive development, and how mutations that disrupt this process lead to developmental disabilities, including ASDs.

The finding that disruption of Ube3A activity leads to a decrease in AMPAR expression at synapses suggests that drugs that promote AMPAR expression at synapses might reverse symptoms associated with AS. Studies of another human disorder, fragile X syndrome (FXS), where a decrease in AMPAR expression at synapses has been observed suggest that this type of therapeutic strategy has potential. In FXS, the decrease in AMPAR expression at synapses is due to excessive mGluR5 signaling, resulting in increased Arc translation and excessive AMPAR internalization (Dölen and Bear, 2008; Park et al, 2008). In a mouse model of FXS, injection of the mGluR5 antagonist MPEP restored surface expression of AMPARs and prevented the symptoms associated with FXS (Dölen et al., 2007; Nakamoto et al., 2007; Yan et al., 2005). These results have led to the development of more specific mGluR5 antagonists that are now entering clinical trials for the treatment of FXS. It is possible that similar approaches will also be effective for treating AS.

A recent study demonstrated that the mutation of an inhibitory phosphorylation site of αCaMKII rescues many behavioral deficits exhibited by Ube3A-deficient mice, suggesting that subtle genetic manipulations can reverse Ube3A loss-of-function phenotypes (van Woerden et al., 2007). An intriguing aspect of this finding is that increasing CamKII activity results in increased AMPAR expression at synapses (Rose et al., 2009) and this may explain why increased CaMKII activity rescues phenotypes associated with the loss of Ube3A.

Although our results provide hope that it will be possible to develop therapies for treating individuals with AS, it is also likely that the defect in AMPAR expression at synapses is not the only thing that has gone awry in AS. For example, it is not obvious how impaired AMPAR receptor function results in an increased susceptibility to seizures and thus it is likely that Ube3A substrates in addition to Arc play roles in nervous system development. In addition, individuals with AS have sleep disturbances, hyperactivity, inappropriate laughter, and movement disorders. Given the broad phenotypic consequences of AS, it is likely that the disruption of the degradation of a number of Ube3A substrates contributes to AS. In the present study, we have defined a Ube3A binding domain that has aided in the identification of new Ube3A substrates. One of these substrates is the RhoGEF ephexin5, which plays an important role in restricting the number of synapses formed by a neuron (S.S. Margolis and M.E.G., unpublished data). We have also identified Sacsin as a Ube3A substrate that is mutated in Charlevoix-Saguenay spastic ataxia, and it is intriguing to speculate that in AS the absence of Ube3A-mediated ubiquitination of Sacsin may contribute to the movement disorders associated with AS. In addition to ephexin5 and Sacsin, we have identified a number of other proteins that contain the UBD. It will be important in the future to determine how these substrates work together with Ube3A to fine tune synapse development.

EXPERIMENTAL PROCEDURES

Cell Cultures, Transfections, and Infections

HEK293T cells and hippocampal neurons were cultured, transfected, and infected as previously described (Flavell et al., 2006). Organotypic slice cultures were prepared from P3-6 rat or mouse brains, and 350 μm slices of hippocampus were prepared and transfected as described previously (Zhou

et al., 2006). Acute slices were prepared from P15–18 mice as described previously (Lin et al., 2008).

Mice

Ube3A knockout mice were obtained from The Jackson Laboratory, strain 129- *Ube3a*^{tm1Alb}/J, from stock number 004477. HA-ubiquitin mice were previously described (Ryu et al., 2007). Seizure and enriched environment experiments were carried as described in the Extended Experimental Procedures.

Quantitative Real-Time PCR

PCR was carried out according to standard procedures. Specific primers are listed in the Extended Experimental Procedures.

Chromatin Immunoprecipitation

Details of the chromatin immunoprecipitation and the primers used are described in the Extended Experimental Procedures.

Image Analysis

Images were acquired on a Zeiss LSM5 Pascal confocal microscope and spine and synapse analysis was performed as previously described (see the Extended Experimental Procedures).

Plasmids

Details of plasmid preparation are available in the Extended Experimental Procedures.

Ubiquitination Assay and In Vitro Binding

Two micrograms of Arc C-terminal protein (132–396 aa) was incubated with 2 μg of GST-WT or mutant Ube3A (C833A) in binding buffer (20 mM Tris-HCL [pH 7.4], 50 mM NaCl, 4 mM ATP, 10 mM MgCl2, 0.2 mM dithiothreitol, and 1% Triton X-100). After 2 hr of mixing at 4°C, glutathione-Sepharose beads (GE Healthcare) were added and incubated for another 2 hr. The beads were washed twice with PBS + 1% Triton X-100 and twice with PBS. Proteins were eluted with SDS sample buffer and analyzed by western blotting. For in vitro ubiquitination assays, 1 μg Arc C-terminal protein was incubated with 50 ng E1, 100 ng UbcH7, 200 ng each of WT or mutant (C833A) Ube3A, and 4 μg ubiquitin (BostonBiochem) in 20 mM Tris-HCL (pH 7.4), 50 mM NaCl, 4 mM ATP, 10 mM $MgCl_2$, and 0.2 mM dithiothreitol. Reactions were terminated after 2 hr at 30°C by the addition of SDS sample buffer and were analyzed by western blotting.

Surface GluR1 Staining

Immunostaining of surface GluR1 receptors was performed as previously described (Chowdhury et al., 2006).

Electrophysiology

Electrophysiology was performed using standard methods (see the Extended Experimental Procedures for more detail).

Ube3A Knockout Cultures

Hippocampal cultures were prepared from Ube3A knockout and wild-type littermate mice at P2 using a protocol adopted from K. Condon and M. Ehlers. In brief, hippocampi were dissected in Dissociation Media (DM) (0.3% BSA, 12 mM $MgSO_4$, 10 mM HEPES, 0.6% glucose in Hank's Balanced Salt Solution). Hippocampi were then placed in a papain solution 30 Units/mL in DM for 15 min before resuspension in Neurobasal Medium. The cells were then plated on glass coverslips that had been coated overnight with PDL.

Array Tomography

Array tomography was performed as described (Micheva and Smith, 2007) with modifications as described in the Extended Experimental Procedures.

SUPPLEMENTAL INFORMATION

Supplemental Information includes Extended Experimental Procedures and seven figures and can be found with this article online at doi:10.1016/j.cell.2010.01.026.

ACKNOWLEDGMENTS

We thank S. Margolis for sharing unpublished results and C. Chen, J. Zieg, and S. Cohen for helpful discussions; J. Zieg for assistance with figure making; K. Condon and M. Ehlers for their generous advice on culturing Ube3A knockout neurons; R. Greenberg for assistance with enriched environment experiments; and E. Bennechi for sectioning array tomography ribbons. This research was supported by a National Science Foundation predoctoral fellowship (P.L.G), a Human Frontier Science Program Fellowship (R.H.), a grant from the National Institute of Mental Health (MH53608 to P.F.W), an AS Foundation grant during the initial stages of this work, and a National Institutes of Health grant (NS28829) (M.E.G).

Received: May 15, 2009
Revised: November 9, 2009
Accepted: January 13, 2010
Published: March 4, 2010

REFERENCES

Albrecht, U., Sutcliffe, J.S., Cattanach, B.M., Beechey, C.V., Armstrong, D., Eichele, G., and Beaudet, A.L. (1997). Imprinted expression of the murine Angelman syndrome gene, Ube3a, in hippocampal and Purkinje neurons. Nat. Genet. *17*, 75–78.

Chen, W.G., Chang, Q., Lin, Y., Meissner, A., West, A.E., Griffith, E.C., Jaenisch, R., and Greenberg, M.E. (2003). Derepression of BDNF transcription involves calcium-dependent phosphorylation of MeCP2. Science *302*, 885–889.

Chowdhury, S., Shepherd, J.D., Okuno, H., Lyford, G., Petralia, R.S., Plath, N., Kuhl, D., Huganir, R.L., and Worley, P.F. (2006). Arc/Arg3.1 interacts with the endocytic machinery to regulate AMPA receptor trafficking. Neuron *52*, 445–459.

Clayton-Smith, J., and Laan, L. (2003). Angelman syndrome: a review of the clinical and genetic aspects. J. Med. Genet. *40*, 87–95.

Cook, E.H., Jr., Lindgren, V., Leventhal, B.L., Courchesne, R., Lincoln, A., Shulman, C., Lord, C., and Courchesne, E. (1997). Autism or atypical autism in maternally but not paternally derived proximal 15q duplication. Am. J. Hum. Genet. *60*, 928–934.

Cooper, E.M., Hudson, A.W., Amos, J., Wagstaff, J., and Howley, P.M. (2004). Biochemical analysis of Angelman syndrome-associated mutations in the E3 ubiquitin ligase E6-associated protein. J. Biol. Chem. *279*, 41208–41217.

Dölen, G., and Bear, M.F. (2008). Role for metabotropic glutamate receptor 5 (mGluR5) in the pathogenesis of fragile X syndrome. J. Physiol. *586*, 1503–1508.

Dölen, G., Osterweil, E., Rao, B.S., Smith, G.B., Auerbach, B.D., Chattarji, S., and Bear, M.F. (2007). Correction of fragile X syndrome in mice. Neuron *56*, 955–962.

Engert, J.C., Bérubé, P., Mercier, J., Doré, C., Lepage, P., Ge, B., Bouchard, J.P., Mathieu, J., Melançon, S.B., Schalling, M., et al. (2000). ARSACS, a spastic ataxia common in northeastern Québec, is caused by mutations in a new gene encoding an 11.5-kb ORF. Nat. Genet. *24*, 120–125.

Flavell, S.W., Cowan, C.W., Kim, T.K., Greer, P.L., Lin, Y., Paradis, S., Griffith, E.C., Hu, L.S., Chen, C., and Greenberg, M.E. (2006). Activity-dependent regulation of MEF2 transcription factors suppresses excitatory synapse number. Science *311*, 1008–1012.

Flavell, S.W., Kim, T.K., Gray, J.M., Harmin, D.A., Hemberg, M., Hong, E.J., Markenscoff-Papadimitriou, E., Bear, D.M., and Greenberg, M.E. (2008). Genome-wide analysis of MEF2 transcriptional program reveals synaptic target genes and neuronal activity-dependent polyadenylation site selection. Neuron *60*, 1022–1038.

Gilfillan, G.D., Selmer, K.K., Roxrud, I., Smith, R., Kyllerman, M., Eiklid, K., Kroken, M., Mattingsdal, M., Egeland, T., Stenmark, H., et al. (2008). SLC9A6 mutations cause X-linked mental retardation, microcephaly, epilepsy,

and ataxia, a phenotype mimicking Angelman syndrome. Am. J. Hum. Genet. *82*, 1003–1010.

Glessner, J.T., Wang, K., Cai, G., Korvatska, O., Kim, C.E., Wood, S., Zhang, H., Estes, A., Brune, C.W., Bradfield, J.P., et al. (2009). Autism genome-wide copy number variation reveals ubiquitin and neuronal genes. Nature *459*, 569–573.

Greer, P.L., and Greenberg, M.E. (2008). From synapse to nucleus: calcium-dependent gene transcription in the control of synapse development and function. Neuron *59*, 846–860.

Jiang, Y.H., Armstrong, D., Albrecht, U., Atkins, C.M., Noebels, J.L., Eichele, G., Sweatt, J.D., and Beaudet, A.L. (1998). Mutation of the Angelman ubiquitin ligase in mice causes increased cytoplasmic p53 and deficits of contextual learning and long-term potentiation. Neuron *21*, 799–811.

Kamionka, M., and Feigon, J. (2004). Structure of the XPC binding domain of hHR23A reveals hydrophobic patches for protein interaction. Protein Sci. *13*, 2370–2377.

Kessels, H.W., and Malinow, R. (2009). Synaptic AMPA receptor plasticity and behavior. Neuron *61*, 340–350.

Kishino, T., Lalande, M., and Wagstaff, J. (1997). UBE3A/E6-AP mutations cause Angelman syndrome. Nat. Genet. *15*, 70–73.

Kumar, S., Talis, A.L., and Howley, P.M. (1999). Identification of HHR23A as a substrate for E6-associated protein-mediated ubiquitination. J. Biol. Chem. *274*, 18785–18792.

Lin, Y., Bloodgood, B.L., Hauser, J.L., Lapan, A.D., Koon, A.C., Kim, T.K., Hu, L.S., Malik, A.N., and Greenberg, M.E. (2008). Activity-dependent regulation of inhibitory synapse development by Npas4. Nature *455*, 1198–1204.

Man, H.Y., Sekine-Aizawa, Y., and Huganir, R.L. (2007). Regulation of alpha-amino-3-hydroxy-5-methyl-4-isoxazolepropionic acid receptor trafficking through PKA phosphorylation of the Glu receptor 1 subunit. Proc. Natl. Acad. Sci. USA *104*, 3579–3584.

Matsuura, T., Sutcliffe, J.S., Fang, P., Galjaard, R.J., Jiang, Y.H., Benton, C.S., Rommens, J.M., and Beaudet, A.L. (1997). De novo truncating mutations in E6-AP ubiquitin-protein ligase gene (UBE3A) in Angelman syndrome. Nat. Genet. *15*, 74–77.

Micheva, K.D., and Smith, S.J. (2007). Array tomography: a new tool for imaging the molecular architecture and ultrastructure of neural circuits. Neuron *55*, 25–36.

Miura, K., Kishino, T., Li, E., Webber, H., Dikkes, P., Holmes, G.L., and Wagstaff, J. (2002). Neurobehavioral and electroencephalographic abnormalities in Ube3a maternal-deficient mice. Neurobiol. Dis. *9*, 149–159.

Morrow, E.M., Yoo, S.Y., Flavell, S.W., Kim, T.K., Lin, Y., Hill, R.S., Mukaddes, N.M., Balkhy, S., Gascon, G., Hashmi, A., et al. (2008). Identifying autism loci and genes by tracing recent shared ancestry. Science *321*, 218–223.

Nakamoto, M., Nalavadi, V., Epstein, M.P., Narayanan, U., Bassell, G.J., and Warren, S.T. (2007). Fragile X mental retardation protein deficiency leads to excessive mGluR5-dependent internalization of AMPA receptors. Proc. Natl. Acad. Sci. USA *104*, 15537–15542.

Newpher, T.M., and Ehlers, M.D. (2008). Glutamate receptor dynamics in dendritic microdomains. Neuron *58*, 472–497.

Paradis, S., Harrar, D.B., Lin, Y., Koon, A.C., Hauser, J.L., Griffith, E.C., Zhu, L., Brass, L.F., Chen, C., and Greenberg, M.E. (2007). An RNAi-based approach identifies molecules required for glutamatergic and GABAergic synapse development. Neuron *53*, 217–232.

Park, S., Park, J.M., Kim, S., Kim, J.A., Shepherd, J.D., Smith-Hicks, C.L., Chowdhury, S., Kaufmann, W., Kuhl, D., Ryazanov, A.G., et al. (2008). Elongation factor 2 and fragile X mental retardation protein control the dynamic translation of Arc/Arg3.1 essential for mGluR-LTD. Neuron *59*, 70–83.

Rial Verde, E.M., Lee-Osbourne, J., Worley, P.F., Malinow, R., and Cline, H.T. (2006). Increased expression of the immediate-early gene arc/arg3.1 reduces AMPA receptor-mediated synaptic transmission. Neuron *52*, 461–474.

Rose, J., Jin, S.X., and Craig, A.M. (2009). Heterosynaptic molecular dynamics: locally induced propagating synaptic accumulation of CaM kinase II. Neuron *61*, 351–358.

Ryu, K.Y., Maehr, R., Gilchrist, C.A., Long, M.A., Bouley, D.M., Mueller, B., Ploegh, H.L., and Kopito, R.R. (2007). The mouse polyubiquitin gene UbC is essential for fetal liver development, cell-cycle progression and stress tolerance. EMBO J. *26*, 2693–2706.

Sharfe, N., Freywald, A., Toro, A., and Roifman, C.M. (2003). Ephrin-A1 induces c-Cbl phosphorylation and EphA receptor down-regulation in T cells. J. Immunol. *170*, 6024–6032.

Scheffner, M., Huibregtse, J.M., Vierstra, R.D., and Howley, P.M. (1993). The HPV-16 E6 and E6-AP complex functions as a ubiquitin-protein ligase in the ubiquitination of p53. Cell *75*, 495–505.

Shepherd, J.D., Rumbaugh, G., Wu, J., Chowdhury, S., Plath, N., Kuhl, D., Huganir, R.L., and Worley, P.F. (2006). Arc/Arg3.1 mediates homeostatic synaptic scaling of AMPA receptors. Neuron *52*, 475–484.

Sutcliffe, J.S., Nurmi, E.L., and Lombroso, P.J. (2003). Genetics of childhood disorders: XLVII. Autism, part 6: duplication and inherited susceptibility of chromosome 15q11-q13 genes in autism. J. Am. Acad. Child Adolesc. Psychiatry *42*, 253–256.

van Woerden, G.M., Harris, K.D., Hojjati, M.R., Gustin, R.M., Qiu, S., de Avila Freire, R., Jiang, Y.H., Elgersma, Y., and Weeber, E.J. (2007). Rescue of neurological deficits in a mouse model for Angelman syndrome by reduction of alphaCaMKII inhibitory phosphorylation. Nat. Neurosci. *10*, 280–282.

Williams, C.A., Beaudet, A.L., Clayton-Smith, J., Knoll, J.H., Kyllerman, M., Laan, L.A., Magenis, R.E., Moncla, A., Schinzel, A.A., Summers, J.A., and Wagstaff, J. (2006). Angelman syndrome 2005: updated consensus for diagnostic criteria. Am. J. Med. Genet. A. *140*, 413–418.

Yan, Q.J., Rammal, M., Tranfaglia, M., and Bauchwitz, R.P. (2005). Suppression of two major Fragile X Syndrome mouse model phenotypes by the mGluR5 antagonist MPEP. Neuropharmacology *49*, 1053–1066.

Yashiro, K., Riday, T.T., Condon, K.H., Roberts, A.C., Bernardo, D.R., Prakash, R., Weinberg, R.J., Ehlers, M.D., and Philpot, B.D. (2009). Ube3a is required for experience-dependent maturation of the neocortex. Nat. Neurosci. *12*, 777–783.

Zhou, Z., Hong, E.J., Cohen, S., Zhao, W.N., Ho, H.Y., Schmidt, L., Chen, W.G., Lin, Y., Savner, E., Griffith, E.C., et al. (2006). Brain-specific phosphorylation of MeCP2 regulates activity-dependent Bdnf transcription, dendritic growth, and spine maturation. Neuron *52*, 255–269.

SUPPLEMENTAL EXPERIMENTAL PROCEDURES

Seizures and Enriched Environement

Seizures were induced for three hours in adult CD1 mice by intraperitoneal injection of kainic acid (Ocean Produce International) at a dose of 25 mg/Kg of mouse. For enriched environment experiments, 6 week old CD1 male mice were either placed in standard laboratory cages or in cages containing a variety of rodent toys of various shapes and colors (PETCO) for three hours.

Quantitative Real-Time PCR

Total RNA was harvested from hippocampal neurons at 10 DIV following stimulation with the indicated agent using the RNeasy mini kit (QIAGEN). Stimulants included Bicuculline (Sigma, 20 μM), Glutamate (Sigma, 10 μM), NMDA (Sigma, 20 μM), recombinant human BDNF (Peprotech, 50 ng/mL), NT3 (Peprotech, 50 ng/mL), NT4 (Peprotech, 50 ng/mL), TTX (0.5 μM), CNQX (40 μM), APV (100 μM), and 55 mM KCl as previously described (Chen et al., 2003). Reverse transcription was performed using SuperScript III (QIAGEN), and quantitative RT-PCR using SYBR Green Master Mix was performed on an ABI Prism 7700 according to the manufacturer's instructions. The primers used for this study are listed below:

ArcF: 5′-ACCGTCCCCTCCTCTCTTGA-3′
ArcR: 5′-TCTTTGTAATCCTATTTTCTCTGCCTT-3′
Beta3-tubulinF: 5′-CCCGAGGGCTCAAGATGTC-3′
Beta3-tubulinR: 5′-TCTTTGTAATCCTATTTTCTCTGCCTT-3′
CremF: 5′-AAAGCGGGAGCTGAGGCT-3′
CremR: 5′-TTCTTTCTTCTTCCTGCGACACT-3′
GapdhF: 5′-TCCATGACAACTTTGGCATCGTGG-3′
GaphdhR: 5′-GTTTCTGTTGAAGTCACAGGAGAC-3′
Ube3aF: 5′-TCCTCTTTGGGTGACTCCAG-3′
Ube3aR: 5′-CGGAAGAGAAGCGTAACGAG-3′

Chromatin Immunoprecipitation

Chromatin immunoprecipitation was performed using the ChIP assay kit (Upstate) as previously described (Flavell et al., 2006). The consensus binding site for MEF2 is C/TTAWWWWTAA/G. Primers used for these assays are listed below:

Ube3A promoter 1 F: 5′-GCTCTGGTGGGGAAGACATA-3′
R: 5′-CCAGAAGCAGCACACGAATA-3′
Ube3A promoter 2 F: 5′-AGAAACCTCATAGTGCTTGCAG-3′
R: 5′-TTCTCAACTCTGGCCATCAA-3′
Ube3A promoter 3 F: 5′-TCTGCCCTCTCTACGTCAGG-3′
R: 5′-ATGAAACGAAACCCCACAAG-3′

Image Analysis

Images were acquired on a Zeiss LSM5 Pascal confocal microscope. For spine and synapse analysis, 12-bit images were acquired with a 63X objective at 1024x1024 pixel resolution. Images were acquired using z-stacks of 0.48 μm thickness. Maximum intensity projections were created from the z-stacks and analyzed using MetaMorph image analysis software (Molecular Devices). For each experiment image acquisition and image analysis were performed blinded to genotype and/or condition. Quantification of dendritic spine densities, lengths and widths were obtained manually using MetaMorph software. For all spine measurements at least 200 μm of dendrite was used for each neuron.

Plasmids

pSuper plasmids targeting MEF2A and MEF2D were previously described (Flavell et al., 2006). Bacterial and mammalian expression plasmids of wild-type Ube3A were generously provided by P. M. Howley (Kumar et al., 1999). QuikChange mutagenesis was used to generate Ube3A C833A. Bacterial and mammalian expression plasmids for Arc were previously described (Chowdhury et al., 2006). Arc and Ube3A shRNAs were generated using the pSuper RNAi system (OliogoEngine, Seattle, WA) and the following sequences: Ube3A RNAi #1: 5′- TC**T**CC**A**C**A**G**T**CC**T**GA**AT**AT-3′, Ube3A RNAi #2 5′- CCC**AAT**GA**T**G**T**ATG**A**TCT**A**-3′, Arc RNAi #1 5′AC**C**C**A**A**T**GTGAT**C**CTGCAG-3′, Arc RNAi #2 5′- GC**T**G**AT**GGC**TA**CG**A**C**TA**C**A**-3′ (mismatches listed in bold for scrambled constructs). The following sequences were used to generate RNAi-resistant forms: Ube3Ares #1: TCTGCATAGCCCGGAGTACCTG, Ube3ares#2: TCCGATGATGTACGACCTGAAG, Arcres#1: ACCGAACGTCATACTCCAA, Arc Res#2: GCGGACGGGTATGATTATA.

Quantification of Synapse Density

At 14-18 DIV, cultured hippocampal neurons were fixed in 2% formaldehyde/4% sucrose for 2 min at room temperature and then transferred to 100% methanol for 10 min at −20°C. Coverslips were washed three times with PBS and incubated 1 hr in GDB (0.1% gelatin, 0.3% Triton X-100, 4.2% 0.4 M phosphate buffer, 9% 5M NaCl). Primary antibodies were incubated for 1 hr in GDB at room temperature at the indicated concentrations: PSD-95 (mouse, 1:200; Affinity BioReagents), Synapsin I (rabbit, 1:200; Chemicon), Gad67 (mouse, 1:100; Chemicon), GABAA 2 (rabbit, 1:100, Chemicon). Coverslips were then washed three times with PBS for ten minutes each and then incubated with Cy3- and Cy5-conjugated secondary antibodies (1:300 each; Jackson ImmunoResearch Laboratories) in GDB for one hour at room temperature. Coverslips were then washed three times with PBS for ten minutes each, dipped briefly in water, and mounted on glass slides using Aquamount (Lerner Laboratories). Synapse density was quantified as the overlap of GFP, pre-synaptic marker and post-synaptic marker using Metamorph software and custom macros as previously described (Paradis et al., 2007).

Mass Spectrometry

The sample was separated by SDS-PAGE on a 4%–12% NuPAGE gel (Novex/Invitrogen). The gel band was excised and in-gel digested using trypsin prior to mass spectrometric analysis. All LC/MS experiments were performed by using a LTQ-FT ICR mass spectrometer (Thermo Finnegan, San Jose, CA) coupled to a microscale capillary HPLC (Famos micro-autosampler (LC Packings, Sunnyvale, CA) driven by an Eksigent). Columns were packed in-house by using Magic C18 beads (5 μm particle size, 200 Å pore size; Michrom BioResources, Auburn, CA. Buffer A was 97.3% H_2O/ 2.5% acetonitrile/0.2% formic acid; buffer B was 97.3% acetonitrile /2.5% water/0.2% formic acid; and the loading buffer was buffer A plus 5% formic acid). Data were searched against the mouse IPI database v3.09.fasta using the Paragon and Mascot Algorithms. Mass additions for modifications such as carbamidomethylated cysteine and ubiquitinated lysine were permitted to allow for the detection of these modifications. A confidence score of 99 was required for a peptide for the Paragon algorithm and for Mascot our cutoff score was 40. All modification sites were manually confirmed by interrogating the data.

Acute Slice Preparation

Animals were handled in accordance with Federal guidelines and protocols approved by Children's Hospital, Boston. Hippocampal slices were prepared from wild-type or Ube3A knockout mice between postnatal days 15 and18 (P15–P18). Animals were deeply anesthetized by inhalation of isoflurane. The cerebral hemispheres were quickly removed and placed into ice cold choline-based artificial cerebrospinal fluid (choline ACSF) containing (in mM): 110 choline chloride, 25 NaHCO3, 1.25 NaH2PO4, 2.5 KCl, 7 MgCl2, 25 glucose, 1 CaCl2, 11.6 ascorbic acid, and 3.1 pyruvic acid, and equilibrated with 95% O2/5% CO2. Tissue was blocked and transferred into a slicing chamber containing choline-ACSF. Transverse hippocampal slices (300 μm) were cut with a Leica VT1000s (Leica Instruments, Nussloch, Germany) and transferred into a holding chamber containing ACSF consisting of 127 mM NaCl, 2.5 mM KCl, 25 mM NaHCO3, 1.25 mM NaH2PO4, 2.0 mM CaCl2, 1.0 mM MgCl2, and 25 mM glucose and were equilibrated with 95% O2/5% CO2. Slices were incubated at 31°C for 30–45 min and then left at room temperature until recordings were performed.

Electrophysiology

Whole-cell recordings were obtained from CA1 pyramidal cells visualized under IR-DIC. mEPSC and mIPSC recordings were performed and analyzed as described previously (Lin et al., 2008). Whole-cell recordings were obtained from CA1 pyramidal cells visualized under IR-DIC. Recording pipettes were pulled from borosilicate glass capillary tubing with filaments to yield tips of 2.5-4.5 MΩ resistance. Spontaneous miniature inhibitory postsynaptic potentials (mIPSC) were recorded with pipettes filled with (in mM): 147 CsCl, 5 Na2- phosphocreatine, 10 HEPES, 2 MgATP, 0.3 Na2GTP, and 1 EGTA. Spontaneous miniature excitatory synaptic potentials (mEPSC) and AMPA/NMDA current ratios were recorded with pipettes filled with (in mM): 120 Cesium Methanesulfonate, 10 HEPES, 4 MgCl2, 4 Na2ATP, 0.4 Na2GTP, 10 Na2-phosphocreatine, and 1 EGTA. Intracellular solutions were adjusted to pH 7.3 with CsOH and were 290-300 mOSM. Inhibitory events were pharmacologically isolated by bath application of tetrototoxin (0.5 μM, Tocris Bioscience, Ellisville, Missouri), (R)-CPP (10 μM, Tocris Bioscience, Ellisville, Missouri), and NBQX disodium salt (10 μM, Tocris Bioscience, Ellisville, Missouri), to antagonize voltage-gate sodium channels (VGSC), NMDA receptors, and AMPA receptors, respectively. Excitatory events were isolated with tetrodotoxin, and picrotoxin (50 μM, Tocris Bioscience, Ellisville, Missouri) to antagonize VGSC and GABAA receptors, respectively. Additionally, cyclothiazide (10 μM, Tocris Bioscience, Ellisville, Missouri) was added to the bath to reduce AMPAR desensitization and facilitate measurement and quantification of mEPSCs. AMPA/NMDA ratios were measured in the presence of picrotoxin. For mIPSC and mEPSC recordings, cells were held at −70 mV; AMPA/NMDA current ratios were measured holding the cell at −70 and +40 mV to assess AMPAR and NMDAR mediated currents, respectively. Data were acquired using Clampex10 software and an Axopatch 200B amplifier. Current traces were filtered at 5 kHz, digitized at 10 kHz, and acquired in 10 s intervals. The cell capacitance, input resistance and series resistance were monitored with a 5mV hyperpolarizing step delivered at the beginning of each sweep. Cells were discarded if the series resistance was greater than 25 MΩ. Data were analyzed in IgorPro 5.05 using custom software modified from Shankar et al., 2007. For mIPSC and mEPSC analyses, the root mean square (RMS) was calculated for the first 150 ms of each trace and the event threshold set to be 1.5 times the RMS. Currents were counted as events if they had a rapid rise time (1.5 pA/ms), an exponential decay ($2 < \tau < 200$ ms, $1 < \tau < 50$ ms for mIPSC and mEPSC, respectively), and crossed the event threshold. Data are displayed as the cumulative distribution of all events recorded from

a given genotype. Statistical significance was determined by randomly selecting 50 events from each cell, pooling events from cells of the same genotype and running a Kolmogorov-Smirnov test on the pooled data. $p < 0.05$ was considered statistically significant. Furthermore, data were randomly resampled and the analysis was repeated > 10 times. For each resampling, $p > 0.05$ for all parameters. For AMPA/NMDA current ratios, an extracellular stimulating electrode was placed in stratum radiatum, approximately 200-300 μm from the patched cell in the direction of CA3. Brief current pulses were delivered (0.2 ms) and the evoked response was measured while holding the cell at −70 and +40 mV. The peak current measured at −70 mV was used in the numerator to represent the AMPAR-mediated response. The current amplitude 50-70 ms after the current peak measured at +40 was used in the denominator to represent the NMDAR-mediated response. Data are displayed as the geometric mean ± SEM. Significance was determined by students t test of the log ratio measured from each cell.; $p < 0.05$ was considered significant.

Western Blotting and Antibodies

For Western blotting, whole rat or mouse brains or cultured cells were collected and homogenized in RIPA buffer (50 mM Tris pH 7.5-8.0, 150 mM NaCl, 1% Triton X-100, 0.5% Sodium Deoxycholate, 0.1% SDS, 5 mM EDTA, 10 mM NaF supplemented with complete protease inhibitor cocktail tablet (Roche)). Samples were boiled for 3-5 min in SDS sample buffer, resolved by SDS PAGE, transferred to nitrocellulose, and immunoblotted. Antibodies specific for Ube3A (Sigma), MEF2D (BD Biosciences), MEF2A (Santa Cruz Biotechnology), Arc (Santa Cruz Biotechnology), HA (Roche), and beta-actin (Abcam) are all commercially available. Antibodies for MeCP2 and phospho MeCP2 (Zhou et al., 2006) as well as Vav2 (Cowan et al., 2005) were previously described.

Array Tomography

Array tomography was performed as described (Micheva and Smith, 2007). In summary, acute hippocampal slices (300 um thick) were fixed in 4% paraformaldyhde for 1 hr at room temperature and embedded in LR White resin using the benchtop protocol. Ribbons of between 30-50 serial 100 nm sections of both WT and Ube3a KO were mounted side by side on subbed glass coverslips. Coverslips were immunostained with anti-SV2 (ms, DSHB, 1:100) and anti-GluR1 (Rb, Millipore, AB1504) or anti-NR1 (Rb, Millipore AB9864, 1:100) antibodies as described. Serial sections were imaged using a Zeiss Imager.Z1 microscope with a Photometrics CoolSNAP HQ2 camera on a PLAN APO 63x/1.4 objective. Tissue volumes were aligned using ImageJ (NIH) with the multistackreg plugin (Brad Busse). Reconstructed tissue volumes were cropped to include only stratum lucidum of CA3 and analyzed in Bitplane Imaris and custom software to count synapses. A synapse was counted if the distance between the center point of an SV2 puncta and a GluR1/NR1 puncta was equal to or less than the sum of the radii of the two puncta plus an empirically determined scaling factor of .15 μm. All experiments were carried out and analyzed blinded to genotype.

SUPPLEMENTAL REFERENCES

Cowan, C.W., Shao, Y.R., Sahin, M., Shamah, S.M., Lin, M.Z., Greer, P.L., Gao, S., Griffith, E.C., Brugge, J.S., and Greenberg, M.E. (2005). Vav family GEFs link activated Ephs to endocytosis and axon guidance. Neuron *46*, 205–217.

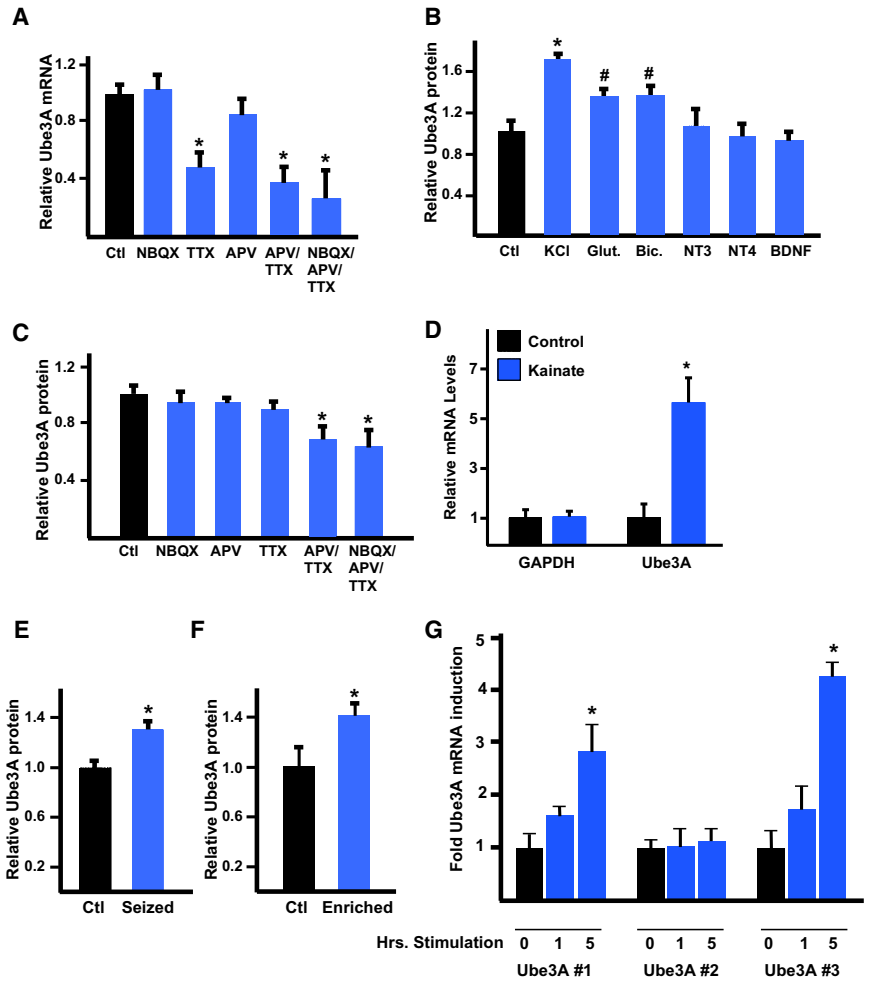

Figure S1. Regulation of Ube3A mRNA and Protein by Neuronal Activity, Related to Figure 1

(A) Real-time PCR analysis of Ube3A mRNA extracted from hippocampal neurons at E18 + 10 DIV treated for six hours with the indicated agent. Data are means +/− SEM from three independent experiments. * indicates statistical significance in pairwise comparison to control: $p < 0.01$ t test.

(B) Quantitative Western blot analysis of Ube3A protein. Protein lysates were collected from hippocampal neurons at E18 + 8 DIV following treatment with the indicated agent for seven hours. This experiment was performed three times independently and the data were normalized to the control and are presented as means +/− SEM. * indicates $p < 0.01$, # indicates $p < 0.05$ in analysis of statistical significance in pairwise comparison to control by t test.

(C) Quantitative Western blot analysis of Ube3A protein. Protein lysates were collected from hippocampal neurons at E18 + 8 DIV following stimulation with the indicated agent for seven hours. This experiment was performed three times independently and the data were normalized to the control and are presented as means +/− SEM. * indicates $p < 0.05$ in analysis of statistical significance in pairwise comparison to control by t test.

(D) Real-time PCR examining Ube3A and GAPDH mRNA levels in extracts from hippocampi of control mice injected with saline (ctl) or mice injected with kainic acid (kainate) to induce seizures. The expression of Ube3A and GAPDH is normalized to the expression of beta-tubulin which serves as an internal standard. Data are presented as mean +/− SEM from three independent experiments. * indicates statistical significance in pairwise comparison: $p < 0.01$ t test.

(E) Quantitative Western blot analysis of Ube3A protein from mice 2.5 hr after injection with saline (ctl) or kainic acid (seized) to induce seizures. Data are presented as mean +/− SEM from three independent experiments. * indicates statistical significance in pairwise comparison $p < 0.05$ t test.

(F) Quantitative Western blot analysis of Ube3A protein from mice housed in standard laboratory cages (control) or placed in cages with novel objects (enriched) for 2.5 hr. Data are presented as mean +/− SEM from three independent experiments. * indicates statistical significance in pairwise comparison $p < 0.05$ t test.

(G) Real-time PCR analysis of the three Ube3A transcripts from mRNA extracted from hippocampal neurons at E18 + 10 DIV stimulated for 0, 1, or 5 hr with 55 mM KCl. Data are presented as mean +/− SEM from three independent experiments. * indicates statistical significance in pairwise comparison: $p < 0.01$ t test.

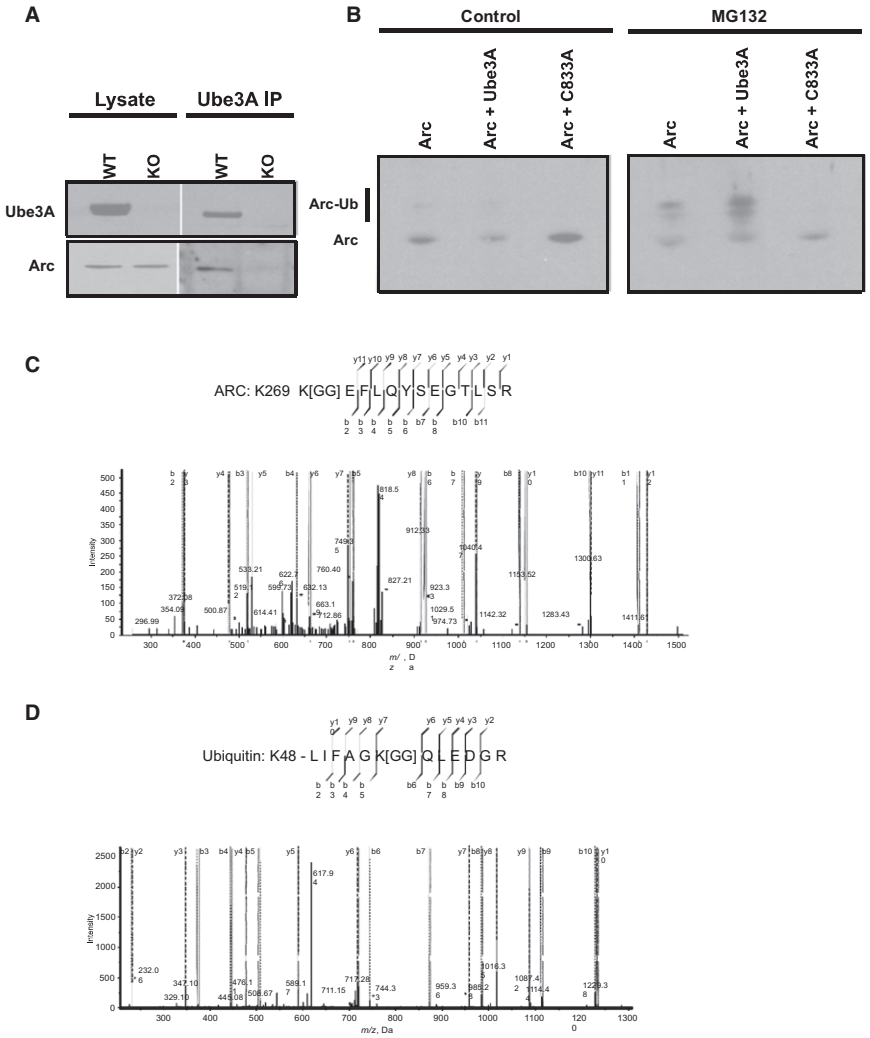

Figure S2. Ube3A Mediates the Polyubiquitination and Degradation of Arc, Related to Figure 3

(A) Western blot analysis of protein lysates made from brains of wild-type and Ube3A knockout mice two hours following kainate acid injection. Immunoprecipitations were performed with an anti-Ube3A antibody and blotted with an anti-Arc antibody to reveal co-immunoprecipitated Arc. Images presented are representative of experiments performed on four independent sets of wild-type and Ube3A knockout mice.

(B) Protein lysates were prepared from HEK293T cells transfected with Myc-Arc and HA-tagged ubiquitin and the indicated constructs and then treated with either vehicle control or the proteasome inhibitor MG132 (10 μM, 8 hr). Arc was then immunoprecipitated using the anti-Myc antibody 9E10, and Western blot analysis was performed using an anti-Arc antibody to reveal both non-ubiquitinated and ubiquitinated forms of Arc.

(C) Mass spectrometric peaks reveal that Ube3A catalyzes the ubiquitination of Arc on lysine 269. Top panel reveals the peptide assigned to the spectra on the bottom. Note the presence of two glycine residues covalently linked to the first lysine of this peptide which is indicative of ubiquitin being attached to that specific residue. The spectra depicted in the bottom panel shows the intensity of peaks on the *y* axis and the mass:charge ratio on the *x* axis. Additional data not pictured here reveal the presence of ubiquitinated lysine 268 as well.

(D) Similar to (C) but this spectra reveals the presence of ubiquitin conjugates on ubiquitin isolated from Arc immunoprecipitates, suggesting that Arc is polyubiquitinated by Ube3A.

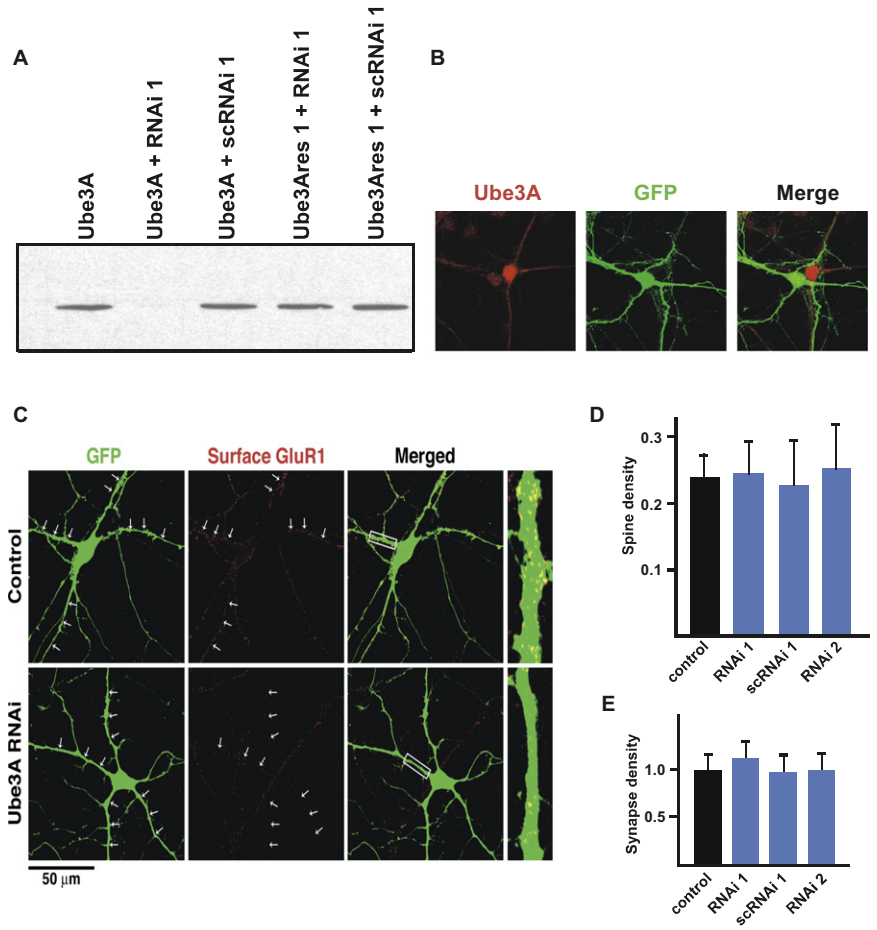

Figure S3. Ube3A RNAi Reduces Ube3A Protein Expression, Related to Figure 4

(A) Western blot analysis of Ube3A from protein lysates prepared from HEK293T cells transfected with the indicated construct(s), using anti-Ube3 antibody.

(B) Representative image of a hippocampal neuron transfected with Ube3A shRNA and GFP. An untransfected neuron in the same field shows Ube3A protein levels in the absence of Ube3A shRNA expression. Red depicts staining with anti-Ube3 antibody, green depicts GFP fluorescence.

(C) Representative images of E18 + 14 DIV hippocampal neurons transfected with GFP and the indicated constructs at 10 DIV and then stained for plasma membrane-expressed GluR1. Arrows mark the dendrites of transfected neurons to make it easier to distinguish the dendrites of transfected from untransfected neurons. The inset on the right is a zoomed in image of the boxed region in the merged panel. Yellow staining is indicative of the presence of GluR1 puncta on the GFP-expressing dendrite of the transfected neuron.

(D) Quantification of dendritic spine density from E18 + 14 DIV hippocampal neurons transfected at 10 DIV with GFP and vector control, either of two shRNAs targeting Ube3A (Ube3A RNAi 1 or 2) or scrambled control shRNA (Ube3A scRNAi 1). Data are presented as mean +/− SEM from three independent experiments.

(E) Quantification of the overlap of PSD95 and synapsin1 puncta on E18 + 14 DIV hippocampal neurons transfected at 10 DIV with GFP and vector control, either of two shRNAs targeting Ube3A (Ube3A RNAi 1 or 2) or scrambled control shRNA (Ube3A scRNAi 1). Data are normalized to control and presented as mean +/− SEM from three independent experiments.

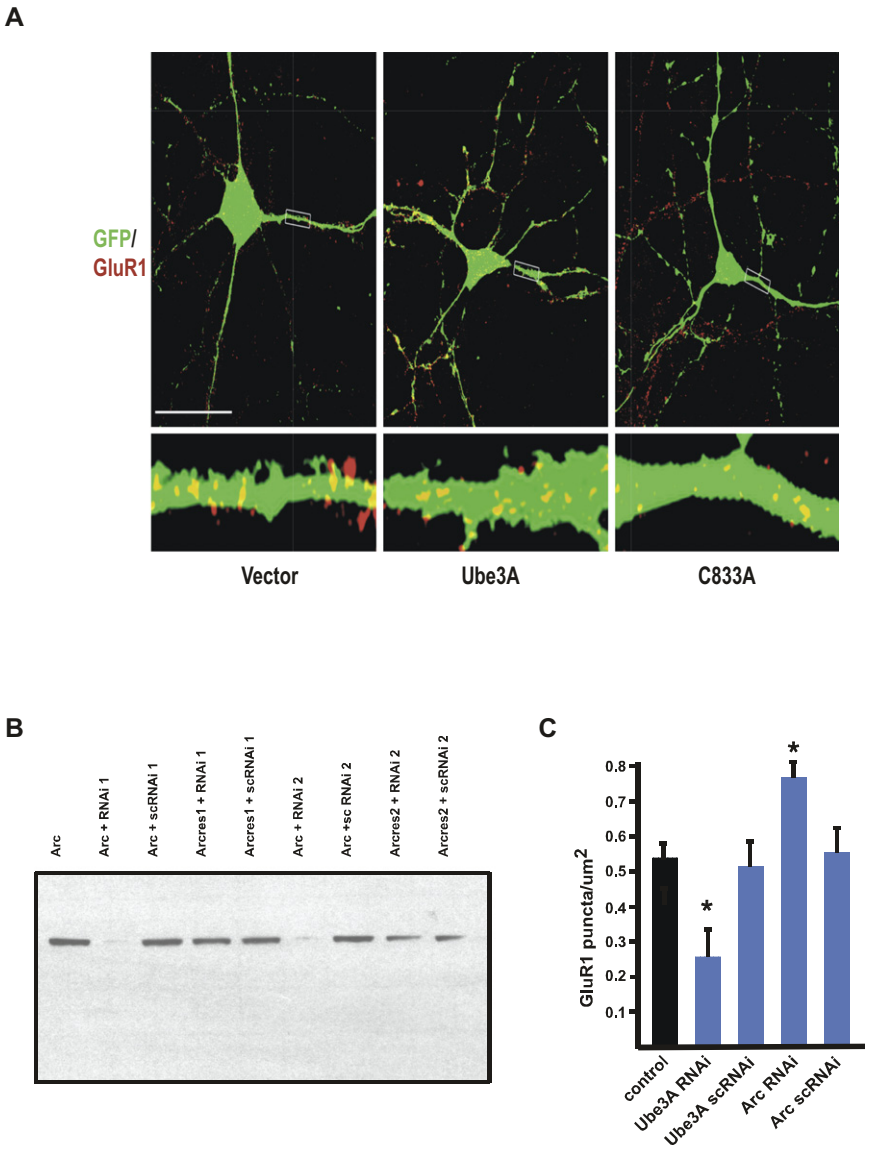

Figure S4. Related to Figure 5

(A) Representative images of surface GluR1 expression from E18 + 17 DIV hippocampal neurons transfected with vector control, Ube3A, or Ube3A C833A. Transfected neurons are indicated in green, and GluR1 staining is depicted in red. Yellow staining is indicative of the presence of GluR1 puncta on the GFP-expressing dendrite of the transfected neuron.

(B) Western blot analysis of extracts from HEK293T cells transfected with Arc alone, or in combination with either of two Arc shRNA constructs (RNAi 1 or 2), either of two control shRNAs (scRNAi 1 or 2), or either of two forms of Arc that are subtly mutated and thus resistant to the shRNAs (Arcres 1 or 2). Western blots were then performed on lysates from the transfected cells using an anti-Arc antibody.

(C) Quantification of surface expression of GluR1 receptors from E18 + 19 DIV hippocampal neurons transfected with GFP and vector control, Ube3A RNAi, Ube3A scRNAi, Arc RNAi, or Arc scRNAi. Data are presented as mean +/− SEM from three independent experiments. * indicates statistical significance $p < 0.05$, ANOVA, with Bonferroni correction for multiple comparison.

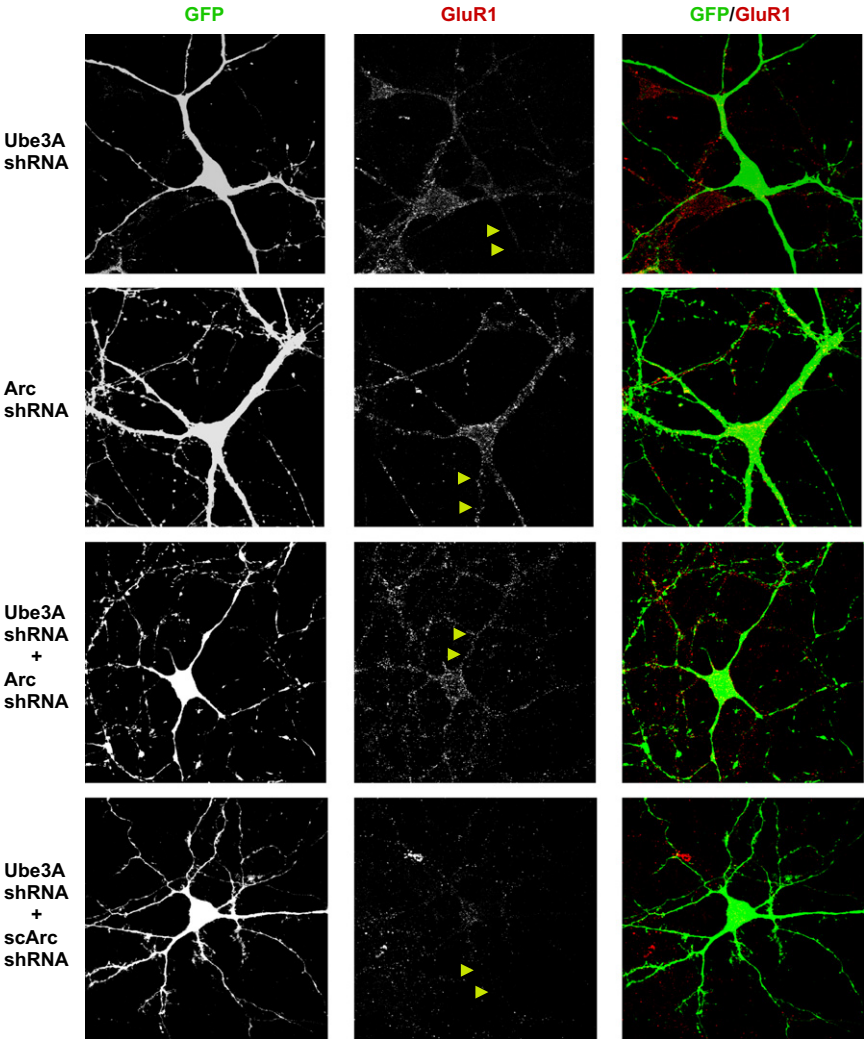

Figure S5. Related to Figure 5

Representative images of surface GluR1 expression from E18 + 16 DIV hippocampal neurons transfected at 10 DIV with Ube3A shRNA, Arc shRNA, Ube3A shRNA + Arc shRNA or Ube3A shRNA + Arc scRNA. Left panels indicate GFP, middle panels indicate surface GluR1 expression, and right panels are composite images of GFP and surface GluR1 staining. Arrows point to transfected dendrites facilitating visualization of surface GluR1 in transfected neurons.

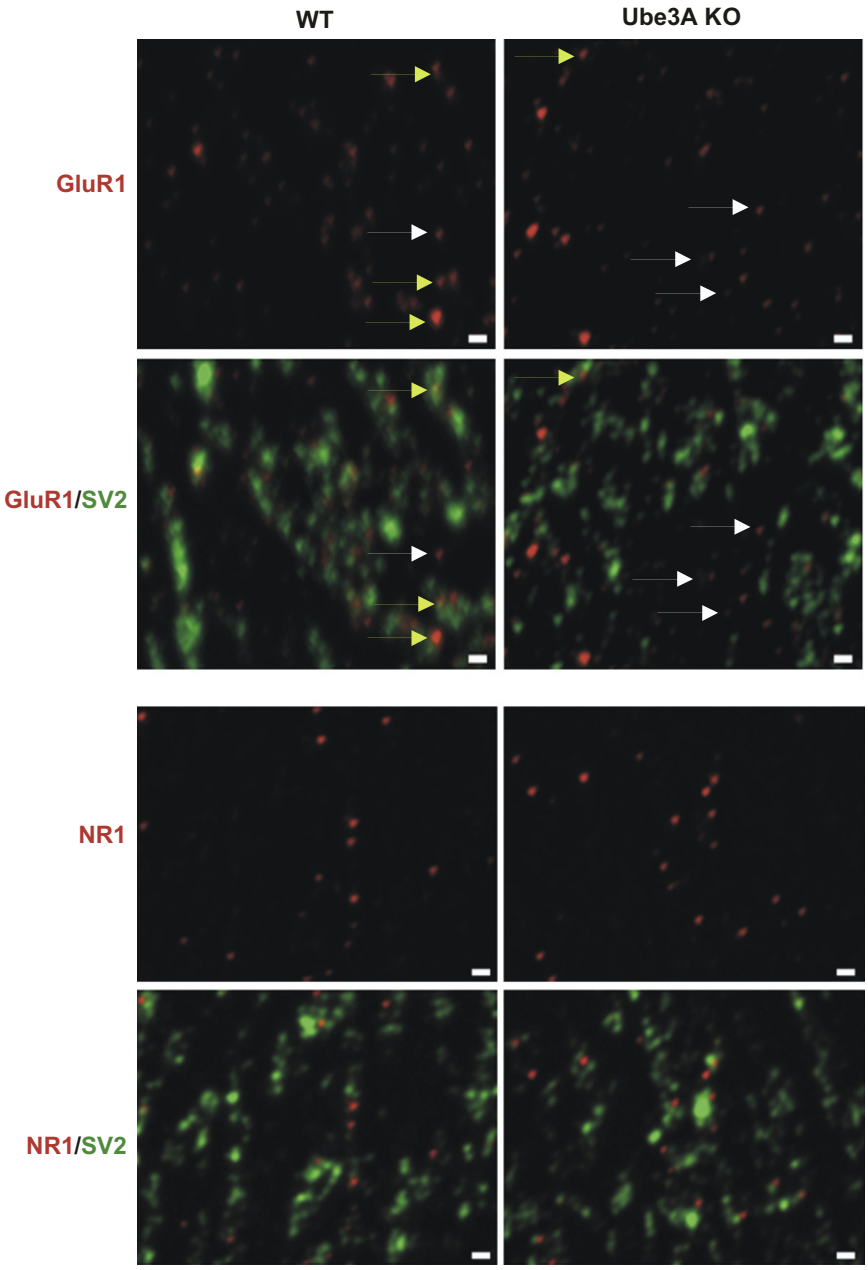

Figure S6. Related to Figure 6

Representative array tomography images obtained from hippocampal sections of P21 Ube3A knockout and wild-type littermates stained with anti-GluR1 and anti-SV2 antibodies (top two panels) or anti-NR1 and anti-SV2 antibodies (bottom two panels). Scale bar represents 1 μm. From the images it can be seen that some GluR1 puncta are in close apposition to SV2 puncta and other GluR1 puncta are not proximal to SV2 puncta (white arrows point to representative GluR1 puncta not associated with SV2 puncta; yellow arrows point to representative GluR1 puncta that are associated with SV2 puncta). The percentage of GluR1 puncta associated with SV2 is significantly higher in wild-type hippocampi compared to Ube3A knockout hippocampi. We would like to note that SV2 is a synaptic vesicle associated protein and as synaptic vesicles are often fairly distant from post-synaptic components, there are a number of SV2 puncta that are not associated with any post-synaptic markers.

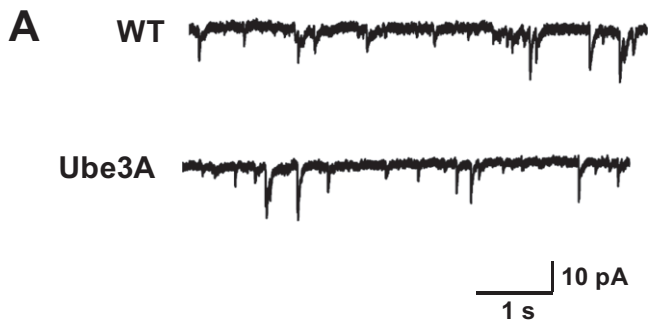

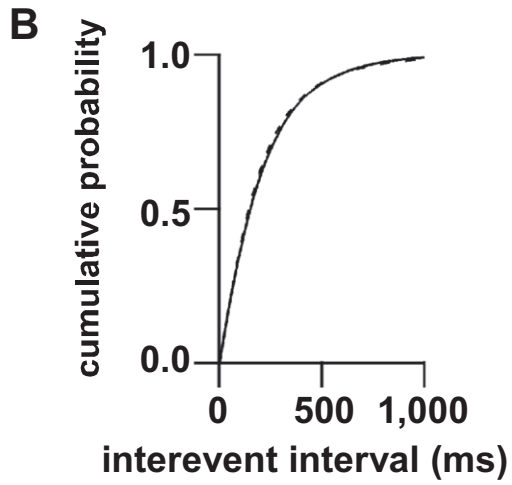

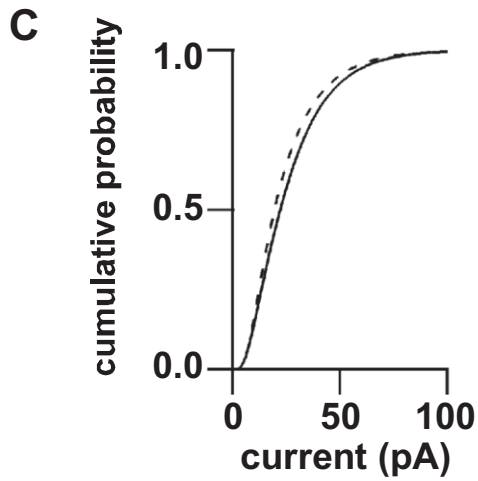

Figure S7. mIPSCs Are Unaltered in Ube3A Knockout Mice, Related to Figure 7

(A) Representative mIPSC traces of hippocampal neurons from wild-type (top) and Ube3A knockout neurons (bottom).

(B) Quantification of mIPSC frequency from wild-type (solid line) and Ube3A knockout (dashed line) mice. Data are presented as cumulative probability plots of interevent intervals and represent recordings from at least 15 neurons from at least three independent animals of each genotype.

(C) Quantification of mIPSC amplitude from wild-type (solid line) and Ube3A knockout (dashed line) mice. Data are presented as cumulative probability plots and represent recordings from at least 15 neurons from at least three independent animals of each genotype.